H. Nabi, T. Lombaerts, Y. Zhang, E. Van Kampen, Q.P. Chu, C.C. De Visser
Effects of Structural Failure on the Safe Flight Envelope of Aircraft
Journal of Guidance Control and Dynamics, Vol. 41, N. 6, 2018, p. 1257-1275
doi:10.2514/1.G003184

Effects of Structural Failure on the Safe Flight Envelope of Aircraft

H. N. Nabi*
Politecnico di Milano, Via La Masa 34, 20156 Milano, Italy

T. Lombaerts†
NASA Ames Research Center, Moffett Field, CA 94035.

Y. Zhang‡, E. van Kampen§, Q. P. Chu¶ and C. C. de Visser‖
Delft University of Technology, Kluyverweg 1, 2629 HS Delft, The Netherlands.

The research presented in this paper focuses on the effects of structural failures on the safe flight envelope of an aircraft, which is the set of all the states in which safe maneuver of the aircraft can be assured. Nonlinear reachability analysis based on an optimal control formulation is performed to estimate the safe flight envelope using actual aircraft control surface inputs. This approach uses the physical model of an aircraft, where the aerodynamic stability and control derivatives are calculated using Digital Datcom. Symmetrical damages to a Cessna Citation II are considered with 25%, 50%, 75% and 100% spanwise vertical tail tip losses, leading to gradual shrinkage in the safe flight envelope. Based on the estimated safe flight envelopes, a discussion on the effects of structural damages and different flight conditions on the safe flight envelope is presented. In particular, the interpolatibility of the resulting safe flight envelopes is demonstrated. This property is essential for a novel database driven flight envelope prediction method; where a database of safe flight envelopes is created offline, later to be accessed in real time.

*PhD Student, Department of Aerospace Science and Technology. hafiznoor.nabi@polimi.it
†Senior Aerospace Research Engineer, Stinger Ghaffarian Technologies, Intelligent Systems Division. thomas.lombaerts@nasa.gov
‡Ph.D. Student, Department of Control and Simulation. Faculty of Aerospace Engineering. y.zhang-9@tudelft.nl
§Assistant Professor, Department of Control and Simulation. Faculty of Aerospace Engineering. e.vankampen@tudelft.nl
¶Associate Professor, Department of Control and Simulation. Faculty of Aerospace Engineering. q.p.chu@tudelft.nl
‖Assistant Professor, Department of Control and Simulation. Faculty of Aerospace Engineering. c.c.devisser@tudelft.nl

Nomenclature

$\mathcal{B}$	=	Set of allowable/achievable states and input vectors
b	=	Wingspan, m
$C_\bullet$	=	Aerodynamic derivatives
$\bar{c}$	=	Mean aerodynamic chord, m
d_x, d_z	=	Perpendicular distance of lost part from new center of gravity, m
$\mathbf{f}$	=	Nonlinear continuous dynamic system
g_1, g_2, g_3	=	Gravity components in wind axes, m/s^2
H	=	Hamiltonian
J	=	Cost function
$J_\bullet$	=	Aircraft mass moment of inertia, kg.m^2
K, L	=	Set of states
l	=	Implicit function
$\ell_{\beta_\bullet}$, $\ell_{r_\bullet}$	=	Parameters of roll moment polynomial model with angle of attack
m	=	Mass of aircraft, kg
$m_{damaged}$	=	Mass of damaged aircraft, kg
$\mathbf{p}$	=	Co-state vector
p, q, r	=	Body angular rates, rad/s
r_z	=	Thrust moment arm in $z-$axis, m
S	=	Wing area, m^2
T	=	Time horizon, s, Total thrust, N
t	=	Time, s
U	=	Set of control inputs
$\mathbf{u}$	=	input vector
V	=	Velocity, m/s
$\mathcal{V}, \mathcal{I}, \mathcal{R}$	=	Viability, invariance and reachability set

V_1, V_2	=	Value function for viability and invariance
$W_\bullet$	=	Weights in cost function
$\mathbf{x}, \dot{\mathbf{x}}$	=	State of the system and time derivative of the state
x, y, h	=	Flat Earth east, Flat Earth north and Altitude, m
$\mathcal{Y}_{p\bullet}$	=	Parameters of side force polynomial model with angle of attack
α	=	Angle of attack, rad
β	=	Sideslip angle, rad
γ	=	Flight path angle, rad
Δ_x, Δ_z	=	Shift in center of gravity, m
$\delta_a, \delta_e, \delta_f\ \delta_r$	=	Aileron, Elevator, Flap and Rudder deflection, rad
$\eta_{p\bullet}, \eta_{\delta_a\bullet}$	=	Parameters of yaw moment polynomial model with angle of attack
ρ	=	Air density, kg/m^3
τ	=	Time instant, s
ϕ	=	State trajectory
ϕ, θ, ψ	=	Euler angles, rad

I. Introduction

Air travel is one of the safest modes of transport. This has been possible due to a continuous focus on aviation safety over the years. A number of studies has been conducted to investigate the causes of in-flight failures and to recommend the necessary steps to prevent such failures in the future. One such study by CAST/ICAO [1] shows that Loss of Control (LOC) in flight was the primary cause of fatal accidents in civil aviation. The study presented a statistical analysis of aircraft accidents during the period of 2006 till 2015 and it is indicated that LOC comprises as much as 23% of all catastrophic aircraft accidents. LOC entails that the aircraft has left the safe flight envelope [2], which is defined as the set of all the states for which the aircraft can be safely maneuvered. Structural damage to the aircraft deteriorates the flying qualities [3], and as a result, the safe flight envelope may *shrink* and the aircraft may find itself outside of this changed safe flight envelope, which leads to LOC.

To prevent LOC, it is very important to have knowledge about the restricted safe flight envelope of an impaired aircraft [4–6], so that it can be ensured that the aircraft does not leave the safe flight envelope. This information can also be used to improve the pilot's overall situation awareness significantly [5, 6].

The flight envelope has been estimated in the literature by means of various methods. The estimation methods include wind tunnel testing, flight experiments and model based computation of achievable trim points [7, 8] or using a vortex lattice algorithm coupled with an extended Kalman filter [9]. A more extensive and rigorous method is to estimate the safe flight envelope by considering it to be a nonlinear reachability problem and to obtain the solution by numerically solving the Hamilton-Jacobi-Bellman (HJB) partial differential equations or Hamilton-Jacobi-Isaacs (HJI) equations when the presence of disturbances is considered in the analysis. Reachability analysis allows a very detailed and accurate estimation of the safe flight envelope, however, the major challenge associated with such an analysis is the "*curse of dimensionality*" [10]. Therefore, it limits the application of available numerical tools for online safe flight envelope estimation to relatively low dimensional problems. To the best of our knowledge, the maximum dimension of the safe flight envelope that has been estimated offline using the reachability analysis is four [11, 12]. Recently, several computationally efficient methods have been explored for flight envelope estimation [13].

To circumvent the "curse of dimensionality" associated with the nonlinear reachability analysis, a database approach toward flight envelope prediction and protection was first introduced by Tang et al. [14], however, the study conducted in this research was only limited to actuator failure scenarios and did not include actual control inputs, rather a "*virtual input*" in the form of angle of attack for the reachability analysis. The same concept has been recently reintroduced [15–17] and extends the implementation of the database approach to structural damages. The basic principle of the database approach is that instead of trying to solve the HJB/HJI equations in real time, a database of safe flight envelopes corresponding to the most often occurring failures is created offline. This offline database is then carried on-board of the aircraft and, when a failure occurs, the database is accessed to obtain the stored safe flight envelopes that are closest to the actual failure. These candidate envelopes are interpolated such that they resemble the actual failure case. The interpolated safe flight envelope is then used by the fault tolerant flight control system to prevent the aircraft from leaving the safe flight envelope, thereby preventing loss of control. Moreover, this information is also displayed to the pilot in order to improve the overall situation awareness. Figure 1 shows an overview of the database approach to flight envelope prediction and protection.

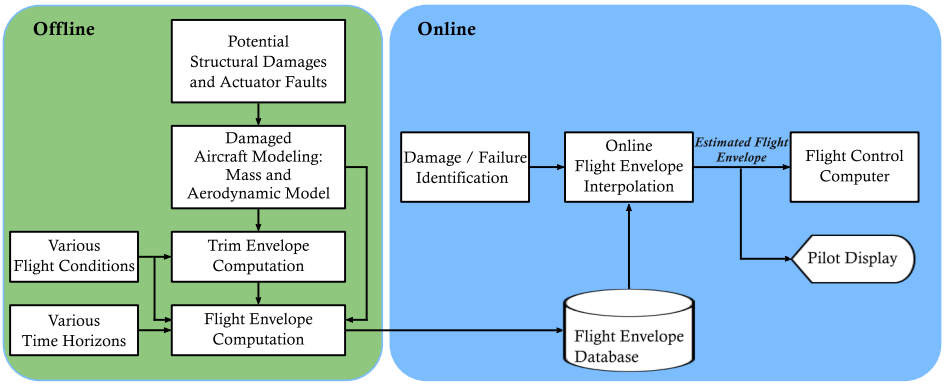

Fig. 1 The database approach with offline (off-board) and online (on-board) segments displayed

The focus of the current paper is on the offline part of the database approach in order to investigate the feasibility of this novel method. The objective is to construct a database of safe flight envelopes corresponding to tip loss (in percentage of span) of the vertical tail at various flight conditions. In particular, the study aims to show how structural failures affect the safe flight envelope of an aircraft and how these effects can be grouped into categories. This information is of great significance for the novel database approach to the real time flight envelope prediction and protection. The main contribution of the current study toward safe flight envelope estimation is that, for the first time, the flight envelope for the damaged aircraft is estimated using realistic control inputs and aerodynamic models.

The paper is arranged into sections as follows: Section II presents a brief introduction of the topics related to the safe flight envelope estimation and the reachability set theory. The curse of dimensionality and the possible solutions to the problem are discussed in section III. An aerodynamic and a mass model of the damaged aircraft is presented in section IV. Sections V and VI present the trim and the safe flight envelopes for the longitudinal and the lateral motion of the aircraft respectively. Lastly, a brief conclusion is presented in section VII.

II. Reachability Set Theory and Safe Flight Envelope

The conventional definition of the flight envelope refers to a region of airspeed and altitude where an aircraft is required to operate or a constrained area in the velocity versus load factor graph [18, 19]. According to this standard definition, only the quasi-stationary aircraft states are considered in defining a flight envelope. In order to incorporate the constraints posed on the envelope by the aircraft's dynamic behavior and for the purpose of avoiding LOC, the safe flight envelope is formally defined as [20]:

The set of aircraft's state space for which the aircraft can be safely controlled and loss of control can easily be avoided.

This set is also referred to as the immediate flight envelope [14] or the dynamic flight envelope [20].

A. Reachability Set Theory

The reachability set theory is widely used in the safety analysis. It studies the behavior of entire sets of trajectories of dynamic systems and determines whether these trajectories can reach a point from another in a given time.

Consider a continuous time system $\dot{\mathbf{x}} = \mathbf{f}(\mathbf{x}, \mathbf{u}, t)$, a time horizon $T \geq 0$, control inputs $\mathbf{u} \in U$ and a set of states K. There are three main sets that can be formulated, associated with the set K and the trajectories that lead to K over a time horizon T [21].

Invariance $\mathcal{I}(t, K)$: Set of all the states $\mathbf{x}(\cdot)$ for which there exist all the inputs $\mathbf{u}(\cdot) \in U_{[0,T]}$ such that $\mathbf{x}(t) \in K$ for all $t \in [0, T]$.

Viability $\mathcal{V}(t, K)$: Set of all the states $\mathbf{x}(\cdot)$ for which there exist at least one input $\mathbf{u}(\cdot) \in U_{[0,T]}$ such that $\mathbf{x}(t) \in K$ for all $t \in [0, T]$.

Reachability $\mathcal{R}(t,K)$: Set of all the states $\mathbf{x}(\cdot)$ for which there exist at least one input $\mathbf{u}(\cdot) \in U_{[0,T]}$ and $t \in [0,T]$ such that $\mathbf{x}(t) \in K$.

By comparing the above sets, it can be stated that:

$$\mathcal{I}(t,K) \subset \mathcal{V}(t,K) \subset \mathcal{R}(t,K) \tag{1}$$

Moreover, the principle of duality relates the reachability set and the invariant set as follows:

$$\mathcal{R}(t,K) = (\mathcal{I}(t,K^c))^c \tag{2}$$

Figure 2 shows an illustration of these three sets. The smallest of these sets, as stated in Eq. 1, is the invariant set. It is the set of states, where all the inputs lead to trajectories that remain inside the trim set K throughout the time horizon T. Next is the viability set, which is the largest subset of the trim set K. It can be seen that there are trajectories extending outside the trim set K, however, there is at least one input that keeps the trajectory inside the trim set over the time horizon T. Lastly, the reachability set consists of all the states within and outside the trim set K for which at least one input $\mathbf{u}(\cdot)$ can bring the trajectory to the target set K within a time $t \in [0,T]$.

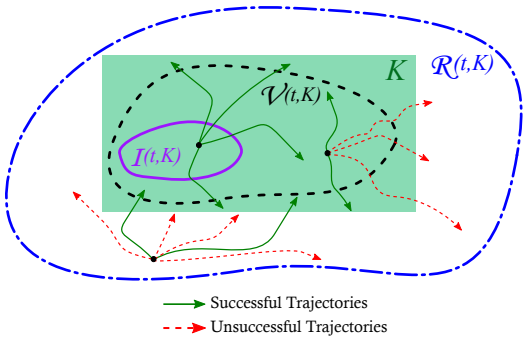

Fig. 2 Invariance (—), viability (- - -) and reachability set (– - –)

The system $\dot{\mathbf{x}} = \mathbf{f}(\mathbf{x},\mathbf{u},t)$ can be evolved forward and backwards in time, which gives two further types of reachability sets; forward and backward reachable sets:

Forward Reachable Set $\mathcal{R}_{\mathcal{F}}(t,K)$: Set of all the states $\mathbf{x}(\cdot)$ for which a control input $\mathbf{u}(\cdot) \in U_{[0,T]}$ exists at time $t \in [0,T]$, such that this set can be approached from at least one point in the trim envelope K.

Backward Reachable Set $\mathcal{R}_{\mathcal{B}}(t,K)$: Set of all the states $\mathbf{x}(\cdot)$ for which a control input $\mathbf{u}(\cdot) \in U_{[0,T]}$ exists at time $t \in [0,T]$, such that at least one state in the trim envelope K can be reached.

The *viability* set and the *invariant* set can be linked to SUPMIN and INFMIN optimal control problems respectively [21]. Suppose that the open set K is associated with the zero level set of a function $l : \mathbb{R}^n \rightarrow \mathbb{R}$ by $K = \{\mathbf{x} \in \mathbb{R}^n \,|\, l(\mathbf{x}) >$

0}, then the viability set can be given as:

$$\mathcal{V}(t,K) = \left\{ \mathbf{x} \in \mathbb{R}^n \,|\, V_1(\mathbf{x},t) = \sup_{\mathbf{u}(\cdot)\in U_{[t,T]}} \min_{\tau\in[t,T]} l\left(\phi\left(\tau,t,\mathbf{x},u(\cdot)\right)\right) > 0 \right\} \tag{3}$$

In the above equation $\phi(\tau,t,\mathbf{x},u(\cdot))$ is the state trajectory. Similarly, assume a closed set L that is associated with the level set of a continuous function $l : \mathbb{R}^n \to \mathbb{R}$ by $L = \{\mathbf{x} \in \mathbb{R}^n \mid l(\mathbf{x}) \geq 0\}$, then the invariant set can be expressed as:

$$\mathcal{I}(t,L) = \left\{ \mathbf{x} \in \mathbb{R}^n \,|\, V_2(\mathbf{x},t) = \inf_{\mathbf{u}(\cdot)\in U_{[t,T]}} \min_{\tau\in[t,T]} l\left(\phi\left(\tau,t,\mathbf{x},u(\cdot)\right)\right) \geq 0 \right\} \tag{4}$$

It is suggested by Lygeros [21], that the characterization of value functions V_1 and V_2, given in Eqs. 3 and 4 respectively, can be represented as viscosity solutions to Hamilton-Jacobi partial differential equations. Hence, the viability set can be written in the form of HJB PDE as:

$$\frac{\partial V_1}{\partial t}(\mathbf{x},t) + \min_{\tau\in[t,T]} \left\{ 0, \sup_{\mathbf{u}(\cdot)\in \mathrm{U}_{[t,T]}} \frac{\partial V_1}{\partial \mathbf{x}}(\mathbf{x},t)\, \mathbf{f}(\mathbf{x},\mathbf{u},t) \right\} = 0 \tag{5}$$

And the invariant set is written in the form of HJB PDE as:

$$\frac{\partial V_2}{\partial t}(\mathbf{x},t) + \min_{\tau\in[t,T]} \left\{ 0, \inf_{\mathbf{u}(\cdot)\in \mathrm{U}_{[t,T]}} \frac{\partial V_2}{\partial \mathbf{x}}(\mathbf{x},t)\, \mathbf{f}(\mathbf{x},\mathbf{u},t) \right\} = 0 \tag{6}$$

The HJB PDE given by Eqs. 5 and 6 can be solved either as an initial value problem or a terminal value problem in order to compute a forward or a backward set respectively. Moreover, the principle of duality as defined by Eq. 2 is used to obtain the reachability set. Eqs. 5 and 6 are solved numerically using the level set toolbox developed in MATLAB® at Stanford University [22, 23], using the algorithm presented by Osher and Fedkiw [24].

B. Safe Flight Envelope as a Reachable Set

The estimation of safe flight envelope as a reachability set problem has been researched in the recent past [12, 14, 20, 21, 25]. This approach with uncertainty quantification and robustness in the estimated values of aerodynamic derivatives is also discussed in detail [26, 27]. The idea is to observe the dynamic behavior of the trim states as they evolve over a certain time horizon T i.e., reachability from the trim envelope. The trim envelope, which is the set of stable and controllable states, is considered as an a-priori safe set. In terms of reachability, the safe flight envelope is defined as the set of states that lie in the intersection of forward and backward reachable sets. The forward reachable set refers to the set of states to which an aircraft can maneuver from the stable trim set. On the other hand, the backward reachable set (or the survivable envelope [27]) refers to the set of states from where an aircraft can recover back to the stable trim set. Hence, the safe flight envelope is the intersection between the aircraft's capability to maneuver from

the trim set and the ability of the aircraft to come back to the trim set. This is illustrated in Figure 3.

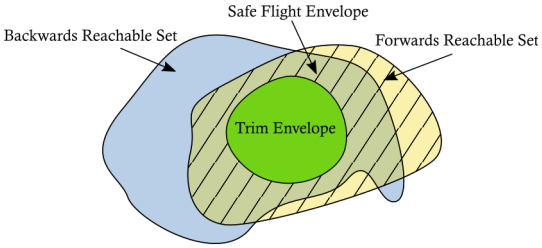

Fig. 3 Safe flight envelope [20]

Note that it is very important to calculate an accurate trim set in order to obtain a correct reachability set. Any untrimmed state which is part of the initial set will lead to an inaccurate safe flight envelope. Computation of the trim states has been discussed extensively in the existing literature. A common approach to compute the trim set is to minimize a cost function using an iterative numerical optimization routine such that the state derivatives are minimized [28, 29]. The trim solution for six-degree-of-freedom aircraft models has also been computed analytically [30]. The advantage of such an analytical method is that it gives all the possible trim solutions, however, it is limited to aircraft models that are linear in control inputs (thrust and control surface deflection). Interval analysis is used to compute the trim solution for a six degree-of-freedom nonlinear F-16 model in horizontal flight [31]. The interval analysis computes all the possible trim solutions within a search space. Another approach in trim set computation is based on bifurcation and continuation methods [32], where the trim states are obtained as function of the control parameters and the stability of each trim states is evaluated in order to identify the potential bifurcation point.

III. Curse of Dimensionality

Estimating the safe flight envelope as a reachability set using the level set method is computationally expensive; the time and the memory required grow significantly with an increase in the problem's dimension. The computational complexity of the level set method is of the order $O\left(N^{n+1}\right)$, with N being the number of computational grid points and n the dimension of the problem [13]. It has been suggested by Kitsios and Lygeros [10] that the "*curse of dimensionality*" in the reachability analysis can be solved by exploiting the structure of the system dynamics using the principle of timescale separation and solving the reachability problem in a sequential manner; first for the faster dynamics and then for the slower dynamics.

Figure 4 shows the structure of timescale separation implemented for a reachability computation by Kitsios and Lygeros [10]. First, the range of pseudo-controls (V, γ) is computed by defining the reachability problem for the faster dynamics. In the next step, the viability set for the states with slower dynamics (x, y, h, ψ) has been estimated using the pseudo-controls (V, γ) and the actual optimal inputs (C_L, ϕ). This allows solving the higher dimensional reachability problem in two steps of lower dimensional reachability problems (two and four respectively). However, although the

dynamics have been split into faster and slower dynamics, these six states belong to the low bandwidth dynamics and are slower than the states belonging to high bandwidth dynamics, such as body angular rates and aerodynamic angles. The states belonging to fast dynamics will be of interest in case of a structural failure to the aircraft. Moreover, the reachability computation performed by Kitsios and Lygeros did not consider actual control inputs to the system, but rather "*virtual inputs*" in the form of lift coefficient C_L and roll angle ϕ.

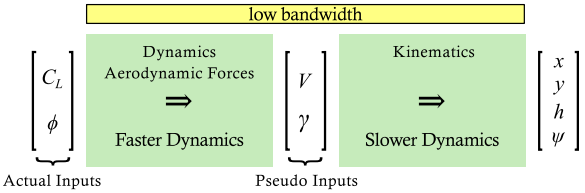

Fig. 4 Time scale separation implemented by Kitsios and Lygeros [10]

Lombaerts et al. [27] has suggested a structure that incorporates faster dynamics and includes actual aircraft control inputs for the reachability computation. This decomposition of aircraft dynamics based on the principle of timescale separation is presented in Figure 5. Note that the fast dynamics has been further decomposed into high and middle bandwidth and these two sets are assumed to be decoupled. However, the suggested sequence of reachability computations for faster dynamics is not feasible when only considering the control surface deflections as inputs for the reachability analysis. Consider the nine-dimensional equations of motion of an aircraft [33]. Firstly, the rotational equations of motion in the body-fixed reference frame are given by:

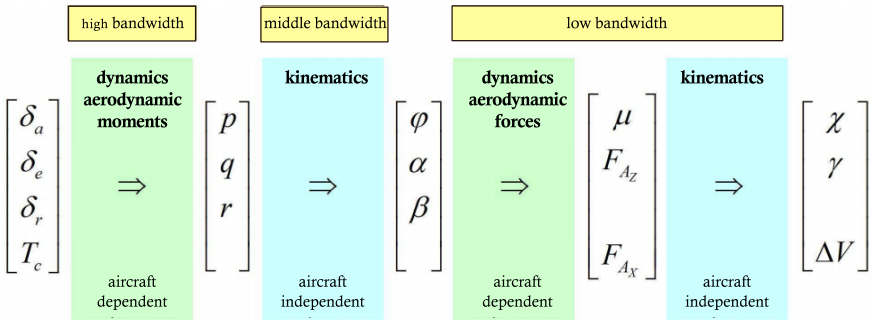

Fig. 5 Time scale separation of aircraft dynamics [27]

$$\begin{cases} \dot{p} = (c_1 r + c_2 p)\, q + c_3 \frac{1}{2}\rho V^2 SbC_l\left(\alpha, \beta, p, r, \delta_a, \delta_r\right) + c_4 \frac{1}{2}\rho V^2 SbC_n\left(\alpha, \beta, p, r, \delta_a, \delta_r\right) \\ \dot{q} = c_5 pr - c_6\left(p^2 - r^2\right) + c_7 \frac{1}{2}\rho V^2 S\bar{c}C_m\left(\alpha, q, \delta_e\right) \\ \dot{r} = (c_8 p - c_2 r)\, q + c_4 \frac{1}{2}\rho V^2 SbC_l\left(\alpha, \beta, p, r, \delta_a, \delta_r\right) + c_9 \frac{1}{2}\rho V^2 SbC_n\left(\alpha, \beta, p, r, \delta_a, \delta_r\right) \end{cases} \tag{7}$$

where the moments of inertia are defined as, with $\Gamma = J_{xx}J_{zz} - J_{zx}^2$:

$$\Gamma c_1 = \left(J_{yy} - J_{zz}\right) J_{zz} - J_{zx}^2 \qquad \Gamma c_4 = J_{zx} \qquad c_7 = \frac{1}{J_{yy}}$$
$$\Gamma c_2 = \left(J_{xx} - J_{yy} + J_{zz}\right) J_{zx} \qquad c_5 = \frac{J_{zz} - J_{xx}}{J_{yy}} \qquad \Gamma c_8 = \left(J_{xx} - J_{yy}\right) J_{xx} + J_{zx}^2$$
$$\Gamma c_3 = J_{zz} \qquad c_6 = \frac{J_{zx}}{J_{yy}} \qquad \Gamma c_9 = J_{xx}$$

Secondly, the force equations of motion in the wind-axes reference frame are:

$$\begin{cases} \dot{V} = \dfrac{1}{m}\left(T\cos\alpha\cos\beta - \frac{1}{2}\rho V^2 S C_D(\alpha) + mg_1\right) \\ \dot{\beta} = p\sin\alpha - r\cos\alpha + \dfrac{1}{mV}\left[-T\cos\alpha\sin\beta + \frac{1}{2}\rho V^2 S C_Y(\alpha,\beta,p,\delta_r) + mg_2\right] \\ \dot{\alpha} = q - p\cos\alpha\tan\beta - r\sin\alpha\tan\beta + \dfrac{1}{mV\cos\beta}\left[-T\sin\alpha - \frac{1}{2}\rho V^2 S C_L(\alpha,q,\delta_f) + mg_3\right] \end{cases} \tag{8}$$

where T is the total thrust and the components of the gravity vector in wind-axes are given by:

$$g_1 = g\left(-\cos\alpha\cos\beta\sin\theta + \sin\beta\sin\phi\cos\theta + \sin\alpha\cos\beta\cos\phi\cos\theta\right)$$
$$g_2 = g\left(\cos\alpha\sin\beta\sin\theta + \cos\beta\sin\phi\cos\theta - \sin\alpha\sin\beta\cos\phi\cos\theta\right)$$
$$g_3 = g\left(\sin\alpha\sin\theta + \cos\alpha\cos\phi\cos\theta\right)$$

And lastly, the kinematic equations are written as:

$$\begin{cases} \dot{\phi} = p + \tan\theta\left(q\sin\phi + r\cos\phi\right) \\ \dot{\theta} = q\cos\phi - r\sin\phi \\ \dot{\psi} = q\frac{\sin\phi}{\cos\theta} + r\frac{\cos\phi}{\cos\theta} \end{cases} \tag{9}$$

From Eqs. 7 and 8, it can be seen that the p, q, r and V, β, α are dependent upon each other. Therefore, the safe flight envelope for angular rates (p, q, r) cannot directly be obtained using the reachability computation without the information about the bounds of the velocity V, sideslip angle β and angle of attack α. Similarly, in order to obtain the safe flight envelope for V, β and α, we need the information about the safe flight envelope for Euler angles (ϕ, θ, ψ) and in order to compute the safe flight envelope for Euler angles, we again require the information of angular rates, see Eq. 9. It can be concluded that, although the principle of timescale separation is useful for the reachability analysis involving slower dynamics as suggested by Kitsios and Lygeros [10], it is not feasible and possible to use the same principle of timescale separation for the faster dynamics. All in all, in order to compute the safe flight envelope of an aircraft using reachability analysis with actual aircraft control inputs alone, a nine-dimensional reachability problem

has to be solved, which is infeasible with current computational implementations.

Estimation of the longitudinal safe flight envelope in a reachability framework using the actual aircraft control inputs (stabilizer deflection and engine thrust) has only been discussed once [12, 20]. Apart from that, in the literature hitherto, reachability computation has been performed for the slower dynamics and therefore, the angle of attack and the sideslip angle etc. have been used as the "*virtual inputs*". However, the changes in the safe flight envelope of these virtual inputs due to a structural damage or a system failure is not considered. In the current paper, the safe flight envelope for the states with fast dynamics has been estimated using the actual control surface inputs.

For the current research, "curse of dimensionality" is addressed by decoupling the dynamics into longitudinal and lateral dynamics. It should be noted, that the decomposition of aircraft dynamics into longitudinal and lateral dynamics is based on the assumption that the aircraft is symmetric ($J_{xy} = J_{yz} = 0$). This assumption will no be longer valid in case of asymmetrical damages and hence the decoupling of flight dynamics into longitudinal and lateral dynamics will not be possible. Therefore, for the current research only symmetrical damages (spanwise damage to the vertical tail) are considered. The spanwise damage to the vertical tail along with different flight conditions, will give a substantial insight into the feasibility of the database approach.

A generalized structure for the safe flight envelope estimation with decoupled dynamics is shown in Figure 6, where the longitudinal envelope can be obtained by using the control surfaces that affect the motion along the longitudinal axis and the lateral envelope is computed using the control surfaces along the lateral axis.

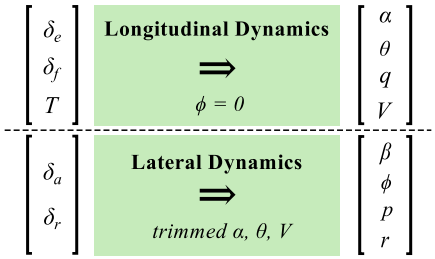

Fig. 6 Safe flight envelope estimation using decoupled dynamics

The longitudinal dynamics is further reduced to a three dimensional problem i.e., $\alpha - \theta - q$ safe flight envelope is computed at a fixed velocity V. Flap and elevator deflections (δ_f, δ_e) are used as inputs for reachability analysis (Eq. 4) and thrust T is varied to keep the velocity constant ($\dot{V} = 0$). Similarly, the lateral dynamics are reduced to a two dimensional problem ($\beta - r$) by considering $p = \phi = 0$. Rudder deflection (δ_r) is used as an input to compute the safe flight envelope and wings are kept level using aileron deflection δ_a.

IV. Modeling of the Damaged Aircraft

Solving the reachability problem using the level set method requires a dynamical model of the system, as indicated by the term $\mathbf{f}(\mathbf{x}, \mathbf{u}, t)$ in Eqs. 5 and 6. One of the key parts of such a dynamic model is the aerodynamic model. In

case of structural damage to an aircraft, the aerodynamic model parameters, in addition to mass and inertial properties of the aircraft, can change. Furthermore, changes in the model structure may also arise due to inertial couplings. The additional parameters that may appear in the model structure of an asymmetrically damaged aircraft can be estimated either by wind tunnel testing or by a Computational Fluid Dynamics (CFD) analysis. A detailed wind tunnel research was conducted at the NASA Langley Research Center in order to study the effects on the aerodynamic model parameters (such as pitching moment coefficient C_m, rolling moment coefficient C_l etc.) of different damage case scenarios to a conventional transport aircraft [34]. Moreover, Bacon and Gregory from NASA Langley Research Center have presented a set of equations of motion for an asymmetrically damaged aircraft [35]. In the current research, however, only symmetrical damages are investigated i.e., spanwise damage to the vertical tail, as mentioned in the previous section. Model parameters for the nominal and the damaged aircraft are calculated using Digital Datcom [36]. The Cessna Citation II laboratory aircraft (PH-LAB), Figure 7, is used as a reference aircraft for the damage modeling.

Fig. 7 Cessna Citation II laboratory aircraft

A. Assumptions

Model of the aircraft is required in order to compute the safe flight envelope. To develop a simple model of the damaged aircraft, certain assumptions are made and are presented as follows:

- The mass of the horizontal tail and the vertical tail is assumed to be 2.5% of the total empty mass of the aircraft and the mass of the dorsal fin is assumed to be 0.5% of the total empty mass of the aircraft.
- x% damage to the vertical tail entails x% loss in the span of the vertical tail and x% loss in the mass of the vertical tail.
- In case of 100% vertical tail loss, it is assumed that the complete tail is lost including horizontal tail and the dorsal fin.
- It is assumed that the damaged part of the vertical tail is a rectangular prism, with thickness equal to the maximum

thickness of the airfoil [37] and that the mass of the lost part is distributed uniformly throughout the rectangular prism

- In Digital Datcom [36], all the distances are measured from the nose of the aircraft. With origin at the nose of the aircraft, the $x-$axis is pointing towards the tail, the $z-$axis is upwards and the direction of $y-$axis completes the right hand rule, see Figure 9.
- Digital Datcom does not provide the rudder control derivatives and hence actual values for the Cessna Citation II obtained from flight data have been used. For the damaged vertical tail, it is assumed that the degradation in control effectiveness of rudder is linear with the damage i.e., $x\%$ loss of vertical tail will lead to $x\%$ degradation in $C_{n_{\delta_r}}$, $C_{l_{\delta_r}}$ and $C_{Y_{\delta_r}}$.

B. Effects of Damage on the Geometry and Mass Properties of the Aircraft

1. Change in Vertical Tail Chord Length

It is assumed that the increase in chord length from tip to root is linear, see Figure 8. Therefore, the tip chord of damaged vertical tail is given by:

$$c_{tip_{damaged}} = \left(\frac{c_{tip_{original}} - c_{root_{original}}}{b_{original}} \right) b_{damaged} + c_{root_{original}} \tag{10}$$

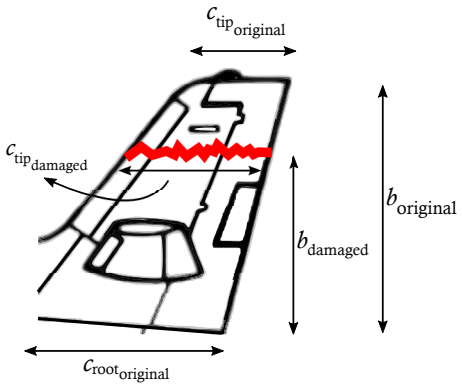

Fig. 8 Vertical tail damage

2. Change in the Mass of the Aircraft

From the second assumption, mentioned in the previous section, the mass of the damaged aircraft is given as follows:

$$m_{damaged} = m_{original} - x\% \cdot m_{VT} \tag{11}$$

In case of 100% vertical tail loss, the mass of the damaged aircraft is then computed as:

$$m_{damaged} = m_{original} - m_{VT} - m_{HT} - m_F \tag{12}$$

where m_{VT} is the vertical tail mass, m_{HT} is the horizontal tail mass and m_F is the mass of the dorsal fin.

3. Change in the Center of Gravity Location

Due to the symmetrical nature of the damage, the movement of center of gravity in $y-$body axis is neglected. Furthermore, it is assumed that the change in center of gravity location is proportional to the loss in mass i.e.,

$$\begin{aligned} x_{c.g.damaged} &= \left(\frac{m_{damaged}}{m_{original}}\right) x_{c.g.original} \\ z_{c.g.damaged} &= \left(\frac{m_{original}}{m_{damaged}}\right) z_{c.g.original} \end{aligned} \tag{13}$$

The use of different mass ratios is because the center of gravity in $x-$axis is moving towards the nose of the aircraft and is moving away from nose in vertical direction due to the vertical tail damage (Figure 9).

4. Change in the Mass Moments of Inertia

Changes in the moments of inertia due to damage are caused by two main factors; 1) change in the position of the center of gravity and 2) change in the mass of the aircraft. Therefore, both of these factors should be taken into account for estimating the modified moment of inertia.

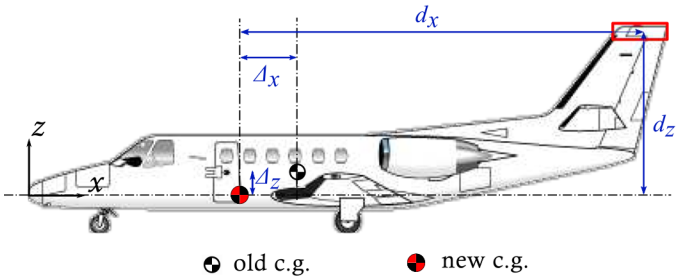

Fig. 9 Center of gravity shift due to tail damage (exaggerated view)

Referring to Figure 9, the moment of inertia of the damaged aircraft is estimated by the following formula:

$$\begin{aligned} &J_{i_{damaged}} = J_{i_{original}} + m_{damaged}\Delta_j{}^2 - (J_{i_{LostPart}} + m_{LostPart}d_j{}^2) \\ &\text{where} \quad i = xx, yy, zz \quad \text{and} \quad j = z, z, x \end{aligned} \tag{14}$$

In the above equation, $m_{damaged}\Delta_j{}^2$ is the correction for the change in the center of gravity location using the parallel

axis theorem. The moment of inertia for the lost part is then subtracted from the overall inertia.

The physical parameters of Cessna Citation II are summarized in Table 1 for the nominal and the damaged aircraft as estimated by methods described above.

Table 1 Physical parameters of Cessna Citation II

Vertical Tail Tip Loss [%]	**0**	**25**	**50**	**75**	**100**
Mass of Aircraft [kg]	5,500	5,477	5,454	5,431	5,299
Tip chord of VT [m]	1.110	1.465	1.820	2.175	–
J_{xx} [kg.m^2]	26,032	25,779	25,622	25,540	25,280
J_{yy} [kg.m^2]	36,388	36,131	35,966	35,869	35,632
J_{zz} [kg.m^2]	59,818	59,131	58,435	57,726	53,556
J_{zx} [kg.m^2]	2,718	2,301	1,971	1,729	791
$x_{c.g.}$ [m]	6.7800	6.7518	6.7237	6.6955	6.5322
$z_{c.g.}$ [m]	-0.0500	-0.0502	-0.0504	-0.0506	-0.0519
Thrust moment arm r_z [m]	0.6784	0.6786	0.6788	0.6790	0.6803
S [m^2]	30				
$\bar{c}$ [m]	2.06				
b [m]	15.9				

C. Effects of Damage on the Aerodynamic Parameters

Aerodynamic effects of the structural damages were calculated using USAF Digital Datcom [36]. Digital Datcom calculates the derivatives of symmetrical aircraft using the methods contained in the USAF Stability and Control Datcom (Data Compendium) [38]. Digital Datcom allows the calculation of static stability, control device and dynamic derivative characteristics of various symmetrical configurations at different flight conditions. Digital Datcom has some operational limitations. One such limitation is that the control derivatives with regards to rudder control surface cannot be obtained by Digital Datcom, as mentioned in the last assumption in section A. Additionally, attached flow is assumed for the estimation of dynamic derivatives and hence is only valid for low angle of attack regime. For further details on Digital Datcom limitations, see section 2.4.5 of Ref. [36].

Based on the aerodynamic parameters that are calculated using Digital Datcom, the following aerodynamic polynomial model is constructed:

$$Longitudinal \begin{cases} C_L = C_{L_0} + C_{L_\alpha}\alpha + C_{L_q}\frac{q\bar{c}}{2V} + C_{L_{\delta_f}}\delta_f \\ C_D = C_{D_0} + C_{D_\alpha}\alpha + C_{D_{\alpha^2}}\alpha^2 \\ C_m = C_{m_0} + C_{m_\alpha}\alpha + C_{m_q}\frac{q\bar{c}}{2V} + C_{m_{\delta_e}}\delta_e \end{cases} \tag{15}$$

$$
Lateral \begin{cases} C_Y = C_{Y_0} + C_{Y_\beta}\beta + (\mathcal{Y}_{p_0} + \mathcal{Y}_{p_\alpha}\alpha)\frac{pb}{2V} + C_{Y_{\delta_r}}\delta_r \\ C_l = C_{l_0} + (\ell_{\beta_0} + \ell_{\beta_\alpha}\alpha)\beta + C_{l_p}\frac{pb}{2V} + (\ell_{r_0} + \ell_{r_\alpha}\alpha)\frac{rb}{2V} + C_{l_{\delta_a}}\delta_a + C_{l_{\delta_r}}\delta_r \\ C_n = C_{n_0} + C_{n_\beta}\beta + (\eta_{p_0} + \eta_{p_\alpha}\alpha)\frac{pb}{2V} + C_{n_r}\frac{rb}{2V} + (\eta_{\delta_{a0}} + \eta_{\delta_{a\alpha}}\alpha)\delta_a + C_{n_{\delta_r}}\delta_r \end{cases} \tag{16}
$$

The last terms in Eq. 16 are the rudder control derivatives and are estimated by the method described in the final assumption in section A. Furthermore, few of the lateral stability derivatives calculated by Digital Datcom vary with the angle of attack. Additional parameters of these lateral stability derivatives for a linear model in angle of attack are defined as follows:

$$
\begin{aligned}
C_{l_\beta} &= \ell_{\beta_0} + \ell_{\beta_\alpha}\alpha \\
C_{l_r} &= \ell_{r_0} + \ell_{r_\alpha}\alpha \\
C_{n_p} &= \eta_{p_0} + \eta_{p_\alpha}\alpha \\
C_{n_{\delta_a}} &= \eta_{\delta_{a_0}} + \eta_{\delta_{a_\alpha}}\alpha \\
C_{Y_p} &= \mathcal{Y}_{p_0} + \mathcal{Y}_{p_\alpha}\alpha
\end{aligned} \tag{17}
$$

Figure 10 shows the geometry of Cessna Citation II as calculated by Digital Datcom. It can be seen in Figure 10(e), that the 100% tail loss include loss in the horizontal tail, vertical tail and dorsal fin, as mentioned in the second assumption in section A.

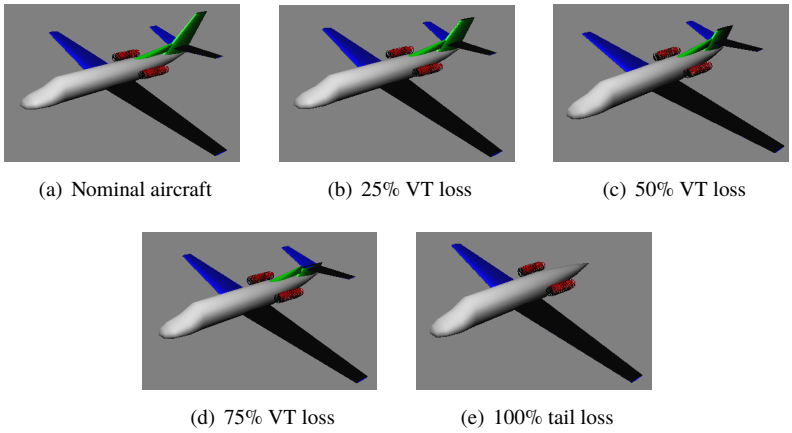

(a) Nominal aircraft (b) 25% VT loss (c) 50% VT loss

(d) 75% VT loss (e) 100% tail loss

Fig. 10 Digital Datcom output of Cessna Citation II

The static and the dynamic stability derivatives that are affected by the vertical tail damage are shown in Figure 11. From the first plot, it can be seen that with 50% loss of the vertical tail, the aircraft is already directionally unstable, which can be seen by the negative slope C_{n_β}. In the second plot, the yaw damping characteristics C_{n_r} exhibit a similar degrading effect throughout the angle of attack range. The third plot shows the variation of the side force coefficient C_Y with the sideslip angle. With the loss in the vertical tail, the sideslip generates less side force compared to the

force generated for nominal aircraft. Roll stability C_{l_β} is also degrading with vertical tail damage. However, there is almost no effect of the vertical tail damage on the roll damping C_{l_r}. Lastly, it is very interesting to look at the C_{m_α} variation with the angle of attack. There is an improvement in the static longitudinal stability with the loss of vertical tail, but as soon as the complete tail is lost, the aircraft becomes longitudinally unstable. The improvement in the static longitudinal stability with spanwise loss in the vertical tail is due to the fact that the center of gravity is moving forward without the reduction of horizontal tail surface area and hence making the aircraft more stable longitudinally; whereas, longitudinal instability with complete tail loss is rather intuitive and self-explanatory.

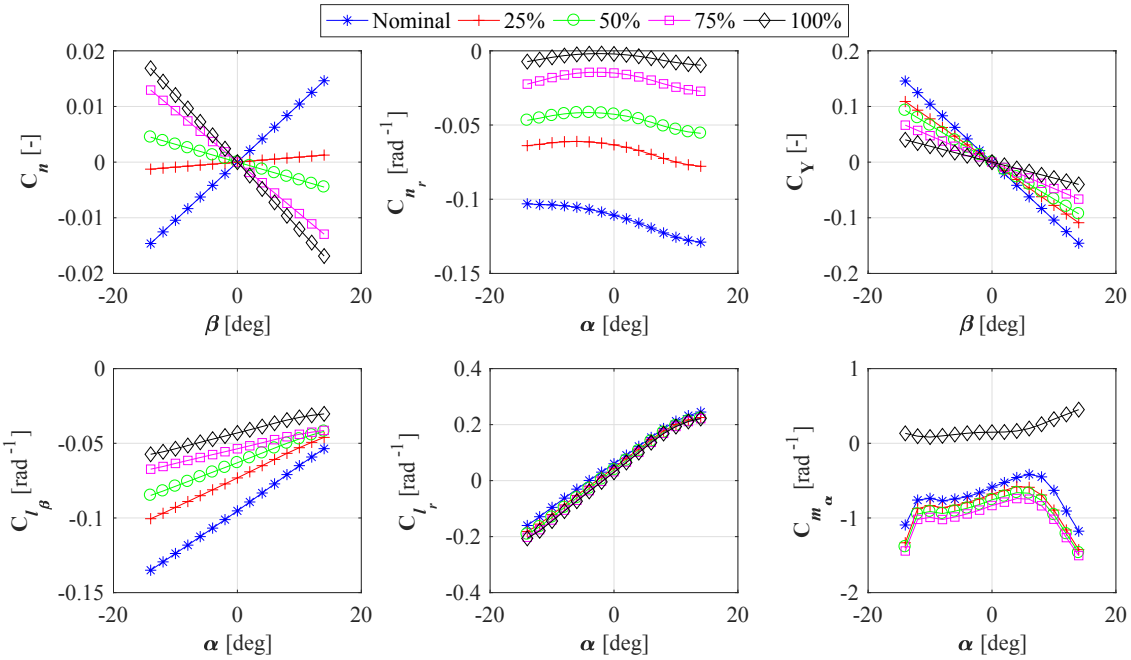

Fig. 11 Effects of vertical tail damage (tip loss in percentage of span) on stability derivatives (obtained from Digital Datcom) at Mach 0.4, sea level

V. Longitudinal Envelope

Longitudinal motion is the motion in the aircraft's plane of symmetry ($x-z$ plane) and is characterized by the state variables: velocity V, angle of attack α, pitch rate q and pitch angle θ. Since the lateral motion is not involved, all the state variables associated with the lateral motion are set to zero i.e.,

$$\beta = \phi = p = r = 0$$

Applying these conditions to the equations of motion described by Eqs. 7, 8 and 9 will result in the longitudinal equations of motion:

$$\begin{cases} \dot{V} = \dfrac{1}{m}\left(T\cos\alpha - \frac{1}{2}\rho V^2 S C_D(\alpha) - mg\sin(\theta-\alpha)\right) \\ \dot{\alpha} = q + \dfrac{1}{mV}\left(-T\sin\alpha - \frac{1}{2}\rho V^2 S C_L(\alpha, q, \delta_f) + mg\cos(\theta-\alpha)\right) \\ \dot{q} = \dfrac{1}{J_{yy}}\left(\frac{1}{2}\rho V^2 S\bar{c} C_m(\alpha, q, \delta_e) - Tr_z\right) \\ \dot{\theta} = q \end{cases} \tag{18}$$

In the above equation total thrust T is assumed to be parallel to $x-$axis in body-fixed reference frame. Furthermore, in the moment equation r_z is the vertical distance between thrust line and body $x-$axis and hence the additional term Tr_z is the pitching moment generated by Thrust. The model structure of aerodynamic coefficients (C_D, C_L, C_m) is given by Eq. 15.

A. Longitudinal Trim Envelope

As described earlier, in order to estimate an accurate safe flight envelope, it is absolutely essential to determine a correct trim envelope. A trim envelope is the set of stable and equilibrium states for which the state derivatives are equal to zero i.e., $\{\mathbf{x}|\mathbf{f}(\mathbf{x},\mathbf{u},t) = 0, (\mathbf{x},\mathbf{u}) \in \mathcal{B}\}$, where $\mathcal{B}$ represents the bound on the control inputs and the allowable states where the model is valid.

The trim envelope is commonly estimated by minimizing a cost function for some fixed states. The cost function for the longitudinal motion that is minimized using the `fminsearch` function of MATLAB® is as follows:

$$J = W_V\dot{V}^2 + W_\alpha\dot{\alpha}^2 + W_q\dot{q}^2 + W_\theta\dot{\theta}^2 \tag{19}$$

In the above equation W_V, W_α, W_q and W_θ are the weights of V, α, q and θ respectively. The aircraft is trimmed at symmetric and generic straight flight at various combinations of angles of attack and pitch angles. A two dimensional grid (α, θ) is set up with constant velocity and zero pitch rate. The thrust is varied to maintain a constant velocity, leaving the flap and the elevator deflections as free parameters that are varied in order to minimize the cost function defined by Eq. 19. Table 2 summarizes the grid setup and the optimization parameters for the estimation of the longitudinal trim envelope for Cessna Citation II. The trim envelope is comprised of only those grid points, for which control inputs are within the bounds and the following conditions are satisfied:

$$\left|\dot{V}\right| \leq 1\times10^{-4}\ [\text{m/s}^2], \quad |\dot{\alpha}| \leq 1\times10^{-4}\ [\text{rad/s}], \quad |\dot{q}| \leq 1\times10^{-4}\ [\text{rad/s}^2], \quad \left|\dot{\theta}\right| \leq 1\times10^{-4}\ [\text{rad/s}] \tag{20}$$

Figure 12 shows the variation of the longitudinal trim envelope with different altitudes at Mach 0.4. As the altitude increases from sea level to 10,000 m, a gradual increase in angle of attack and pitch angle is observed. The increase in

Table 2 Parameters for the longitudinal trim envelope computation

Bounds	Grid Resolution	Cost Function Weights
$T \in [4448.2, 22241]$ [N] $\delta_f \in \left[0, 40\frac{\pi}{180}\right]$ [rad] $\delta_e \in \left[-18\frac{\pi}{180}, 16\frac{\pi}{180}\right]$ [rad] $\alpha \in \left[-14\frac{\pi}{180}, 14\frac{\pi}{180}\right]$ [rad] $\theta \in \left[-30\frac{\pi}{180}, 30\frac{\pi}{180}\right]$ [rad] $q = 0$ [rad/s]	$\alpha_{res} = 0.01$ [rad] $\theta_{res} = 0.055$ [rad]	$W_V = 10$ (for nominal aircraft) $W_V = 0$ (for 100% tail loss) $W_\alpha = W_q = W_\theta = 10$

angle of attack can be explained by the fact that as the altitude increases with constant Mach number, dynamic pressure is decreasing (due to decrease in air density and airspeed). Hence, an increase in the angle of attack is required to maintain the same aerodynamic forces and moment, such that the state derivatives are zero. Moreover, an increase in the angle of attack entails that the pitch angle is also increased in order to keep the gravitational force component constant, see Eq. 18.

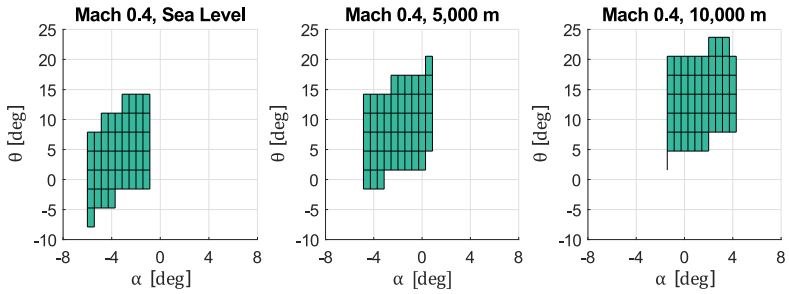

Fig. 12 Variation of longitudinal trim envelope with altitude for nominal Cessna Citation II

Similarly, Figure 13 shows the variation of the longitudinal trim envelope with different Mach numbers at sea level. On this occasion, there is a decrease in angle of attack and pitch angle. This opposite behavior can be explained by the fact that as the Mach number increases from 0.2 to 0.4 at the same altitude, the dynamic pressure increases, and a decrease in the angle of attack is required to maintain the aerodynamic forces and moment. Also, the pitch angle has to be decreased in order to compensate for decreasing angle of attack in the gravitational force term. Figure 14 shows the longitudinal trim envelope at Mach 0.4 at 10,000 m shaded according to the control inputs thrust T, flap deflection δ_f and elevator deflection δ_e.

Lastly, Figure 15 compares the longitudinal trim envelopes for the nominal aircraft and the damaged aircraft with 100% tail loss. The effect of the vertical tail damage alone, does not affect the longitudinal trim envelope significantly and therefore only the longitudinal trim envelope for 100% tail loss scenario is discussed. The conditions imposed by Eq. 20 for the minimization of the cost function defined by Eq. 19 are too strict for trimming the damaged aircraft with 100% tail loss. Therefore, in order to get a sizable trim envelope for the damaged aircraft with no tail, much more

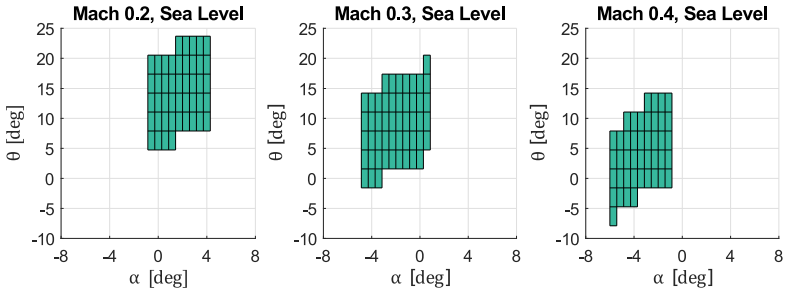

Fig. 13 Variation of longitudinal trim envelope with Mach number for nominal Cessna Citation II

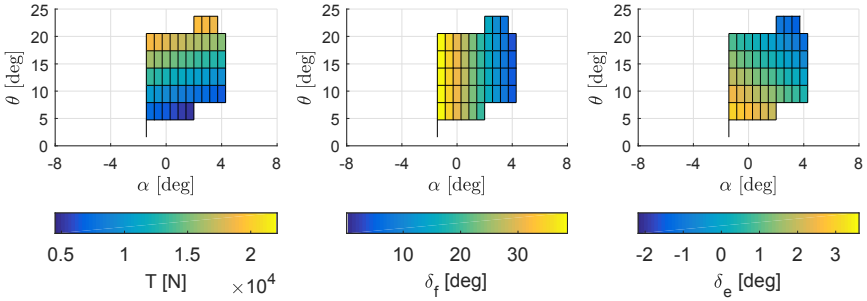

Fig. 14 Longitudinal trim envelope shaded according to control surface deflections at Mach 0.4, 10,000 m

flexible conditions were imposed with $W_V = 0$.

$$\left|\dot{V}\right| \leq 1 \text{ [m/s}^2\text{]}, \quad |\dot{\alpha}| \leq 5 \times 10^{-2} \text{ [rad/s]}, \quad |\dot{q}| \leq 5 \times 10^{-2} \text{ [rad/s}^2\text{]}, \quad \left|\dot{\theta}\right| \leq 5 \times 10^{-2} \text{ [rad/s]} \tag{21}$$

The flexible conditions in the above equation consider accelerations and decelerations, thus does not in fact result in a trim envelope, but rather a pseudo-trim envelope. It can be seen that even with the flexible conditions of Eq. 21, the trim envelope has significantly shrunk. This is expected as the complete horizontal tail is lost including the elevator. Figure 15 also shows the contour plot of the longitudinal pseudo-trim envelope for the damaged Cessna Citation II with 100% tail loss, shaded according to $\dot{V}$. It can be seen that the aircraft accelerates with pitch down and decelerates with pitch up motion. This acceleration and deceleration is due to the flexible condition on $\dot{V}$ as stated in Eq. 21. With almost constant angle of attack, any change in pitch angle will require a change in thrust. However, change in the thrust is limited by the fact that the thrust is generating a pitch down motion. An increase in thrust will cause the aircraft to pitch down, while a decrease in thrust may cause the aircraft to pitch up, and these pitching motions cannot be compensated.

B. Longitudinal Safe Flight Envelope

In section II, the safe flight envelope was defined as the intersection between the forward and the backward reachable sets. The forward or the backward reachable set is computed by solving the HJB equation, Eq. 6, as an initial value

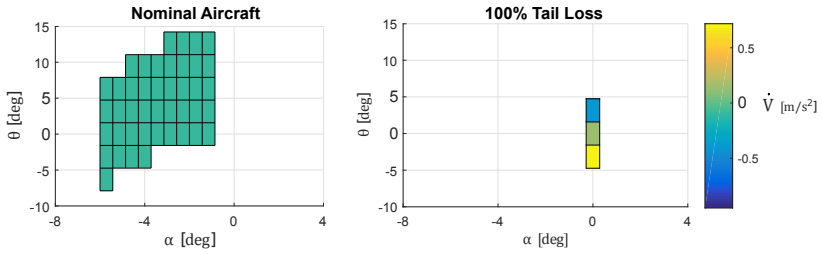

Fig. 15 Comparison of longitudinal trim envelopes for nominal and damaged Cessna Citation II at Mach 0.4, sea level

or a terminal value problem respectively to get the invariant set and then the principle of duality is utilized, Eq. 2, to obtain the reachability set. Eq. 6 is solved using the level set method toolbox [22, 23]. The trim envelope K computed in the previous section is evolved over a time horizon T and is described by the following implicit function:

$$l(\mathbf{x}) = \min\{x_1 - \alpha_{min}, \alpha_{max} - x_1, x_2 - \theta_{min}, \theta_{max} - x_2, x_3 - q_{min}, q_{max} - x_3\} \tag{22}$$

The level set method requires at least one grid point inside the trim set so that the implicit function can be evolved in time to get a meaningful reachable set. However, the longitudinal trim envelope K is a two dimensional plane (α, θ) with $q = 0$ rad/s. Therefore, it is assumed that the states in the near vicinity of $q = 0$ rad/s are also part of the trim set, to be specific $\{q \in K \,|\, |q| \leq 0.01 \text{ rad/s}\}$, which yields an implicit surface defined by Eq. 22. Moreover, it can be noticed that $l(\mathbf{x}) \geq 0$ for $\mathbf{x} \in K$ and $l(\mathbf{x}) < 0$ for $\mathbf{x} \notin K$. Table 3 outlines the parameters that are specified for the reachable set computation.

Table 3 Solver settings for the reachable set computation (longitudinal safe flight envelope)

Parameter	Setting
Computational Domain	$\left[-20\frac{\pi}{180}, 20\frac{\pi}{180}\right]$ rad $\times \left[-45\frac{\pi}{180}, 45\frac{\pi}{180}\right]$ rad $\times \left[-45.8\frac{\pi}{180}, 45.8\frac{\pi}{180}\right]$ rad/s
Number of Grid points	$100 \times 100 \times 100$
Time Horizon	1.0 s

The system defined by the last three equations of Eq. 18 result in a Hamiltonian function of Eq. 6:

$$H(\mathbf{p}, \mathbf{x}, \mathbf{u}) = p_1\dot{\alpha} + p_2\dot{\theta} + p_3\dot{q} \tag{23}$$

where $\mathbf{p}$ in the above equation are the co-states of the value function in Eq. 6: $p_1 = \frac{\partial V_2}{\partial \alpha}$, $p_2 = \frac{\partial V_2}{\partial \theta}$ and $p_3 = \frac{\partial V_2}{\partial q}$. The

quantity to be minimized in the Hamiltonian of Eq. 23 becomes:

$$- p_1 C_{L_{\delta_e}} \delta_e \frac{\rho S}{2m} V - p_1 C_{L_{\delta_f}} \delta_f \frac{\rho S}{2m} V + p_3 C_{m_{\delta_e}} \delta_e \frac{\rho S \bar{c}}{2 J_{yy}} V^2 \tag{24}$$

The minimizers, δ_e and δ_f, depend on the sign of the co-states p_1 and p_3. Recall that $V > 0$ and $C_{L_{\delta_f}} > 0$, then the optimal control inputs for minimizing the Hamiltonian are:

- $\delta_e = \begin{cases} \delta_{e_{\min}} & \text{if } p_3 C_{m_{\delta_e}} \frac{\rho S \bar{c}}{2 J_{yy}} V - p_1 C_{L_{\delta_e}} \frac{\rho S}{2m} > 0 \\ \delta_{e_{\max}} & \text{if } p_3 C_{m_{\delta_e}} \frac{\rho S \bar{c}}{2 J_{yy}} V - p_1 C_{L_{\delta_e}} \frac{\rho S}{2m} < 0 \\ \left[\delta_{e_{\min}}, \delta_{e_{\max}}\right] & \text{if } p_3 C_{m_{\delta_e}} \frac{\rho S \bar{c}}{2 J_{yy}} V - p_1 C_{L_{\delta_e}} \frac{\rho S}{2m} = 0 \end{cases}$
- $\delta_f = \begin{cases} \delta_{f_{\min}} & \text{if } p_1 < 0 \\ \delta_{f_{\max}} & \text{if } p_1 > 0 \\ \left[\delta_{f_{\min}}, \delta_{f_{\max}}\right] & \text{if } p_1 = 0 \end{cases}$

whereas thrust T is varied, such that the velocity V is constant throughout the computational domain of the reachability analysis and is computed by setting the first equation of Eq. 18 to zero and solving for the thrust. The ranges of the control inputs are stated in Table 2.

Figure 16 shows the variation of the safe flight envelope with different Mach numbers at sea level for the time horizon $T = 1$ s. Clearly, with the increasing Mach number, the aircraft's maneuverability increases as shown by the increasing size of the safe flight envelope. Furthermore, it can be seen that there is a noticeable difference between the forward and the backward reachable sets; there are states that can be reached within $T = 1$ s, however, coming back to the trim envelope from the same states is not possible, and vice versa. Another interesting fact to notice here is that the backward reachable set encompasses and extends beyond the computational domain in the $\alpha - q$ plane. Similarly, the forward reachable set at Mach 0.4 at sea level, completely encompasses the $\theta - q$ plane. It is observed that the reachability set extends far from the region, where the linear aerodynamic model and/or structural limits are valid.

The variation of the safe flight envelope with different altitudes at Mach 0.4 is shown in Figure 17. As the altitude increases from sea level to 10,000 m, the safe flight envelope shrinks. With increasing altitude at constant Mach number, density and airspeed decreases and hence the dynamic pressure drops, which makes the aircraft less maneuverable.

The comparison of the safe flight envelopes for the nominal and the damaged Cessna Citation II is presented in Figure 18. An enormous reduction in the size of the safe flight envelope with the complete tail lost is visible. The backward and the forward reachable sets extend in the opposite direction in the $\alpha-$axis. As the elevator is lost, positive pitch angles and pitch rates are not reachable from the trim envelope. On the other hand, thrust is causing the aircraft to pitch down which can be observed by the fact that the forward reachable set is stretching towards negative pitch angles and pitch rates, however, coming back from these negative states is impossible as these states are not part of the

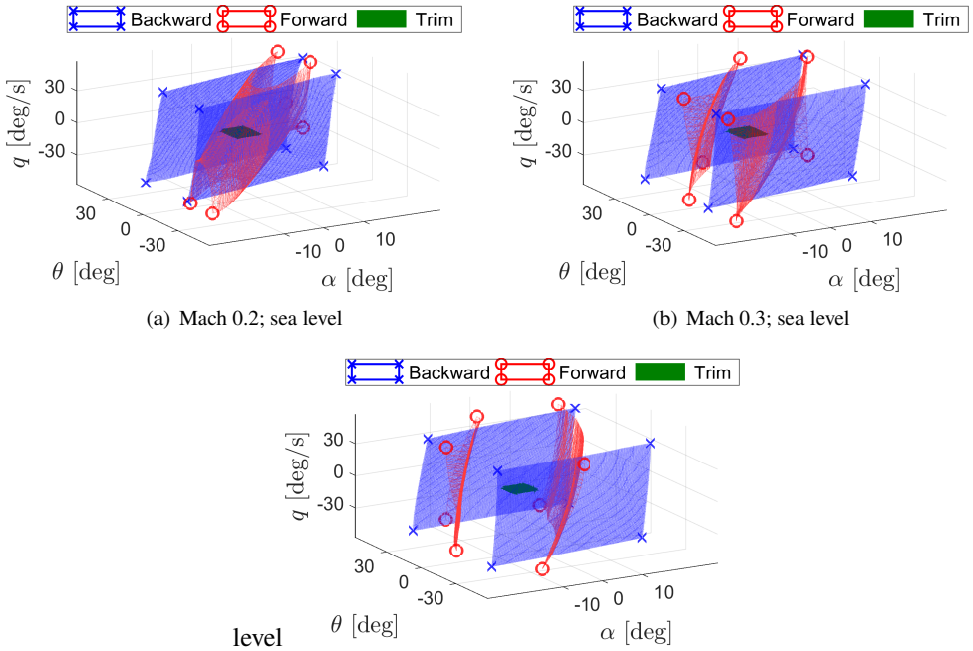

(a) Mach 0.2; sea level

(b) Mach 0.3; sea level

(c) Mach 0.4; sea level

Fig. 16 Longitudinal safe flight envelope for nominal Cessna Citation II with $T = 1$ s (variation with Mach number)

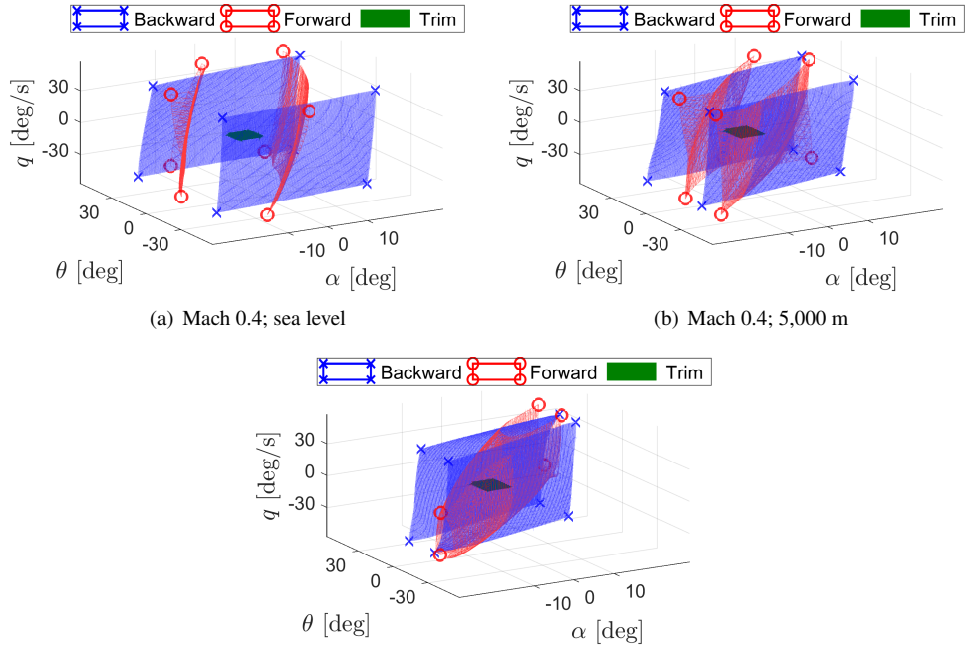

(a) Mach 0.4; sea level

(b) Mach 0.4; 5,000 m

(c) Mach 0.4; 10,000 m

Fig. 17 Longitudinal safe flight envelope for nominal Cessna Citation II with $T = 1$ s (variation with altitude)

backward reachable set. While thrust is fixed in order to maintain the velocity, the only control available is the flap deflection, giving a slight room for maneuverability in the angle of attack.

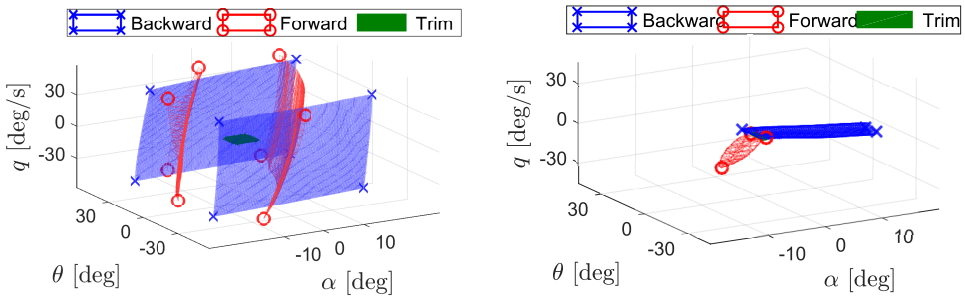

(a) Nominal aircraft (b) 100% tail loss

Fig. 18 Comparison of longitudinal safe flight envelopes for nominal and damaged Cessna Citation II with $T = 1$ s at Mach 0.4, sea level

In order to quantify the change in the size of the safe flight envelopes, number of grid points inside the reachable set as a percentage of total grid points ($100 \times 100 \times 100$) is plotted against different flight conditions and tail damages in Figure 19. As can be seen, that the increase in percentage grid points inside the reachable set (forward and backward) is almost linear with increasing Mach number. Similarly, the decrease in the size of the safe flight envelope is also nearly linear with altitude. Furthermore, the third plot in Figure 19 shows that the reachable sets for the 100% tail damage have shrunk remarkably and the percentage of grid points inside the reachable set has reduced to just 0.11%.

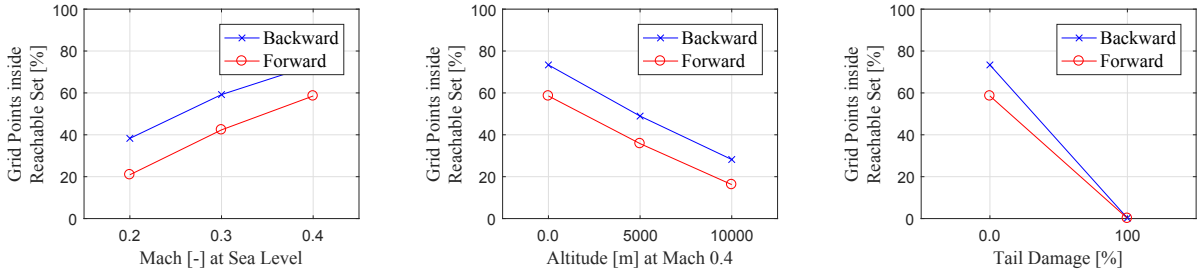

(a) Variation with Mach number (b) Variation with altitude (c) Variation with tail damage

Fig. 19 Change in the percentage of grid points inside the longitudinal reachable set

The computed reachable sets were validated by Monte Carlo analysis. As an example, Figure 20 shows the time evolution of the control inputs and the states for one such Monte Carlo simulation with incremental inputs performed for backward reachable set. The state trajectory is initiated at $(\alpha, \theta, q) = \left(18\frac{\pi}{180} \text{ rad}, 31\frac{\pi}{180} \text{ rad}, 0 \text{ rad/s}\right)$, which lies inside the backward reachable set. As can be seen in the top plot that for the Monte Carlo simulation, the flap and the elevator deflection is randomly changed after each time increment $dt = 0.1$ s, whereas in the second plot the thrust is almost constant, since it is varied to maintain the velocity. The third plot shows the state trajectory itself. The aircraft undergoes extreme maneuvers in order to reach the trim envelope, with state changing at a very high rate i.e., after every 0.1 s. It can be concluded that although the reachability analysis accurately computes the safe flight envelope, many of the states that are part of the "theoretical" reachable set (forward or backward) may not be reachable in reality.

This is due to the fact, that the pilot may not be able to fly such a complex maneuver or the trajectory passes through the states that lie outside the aerodynamic and/or structural limits of the aircraft.

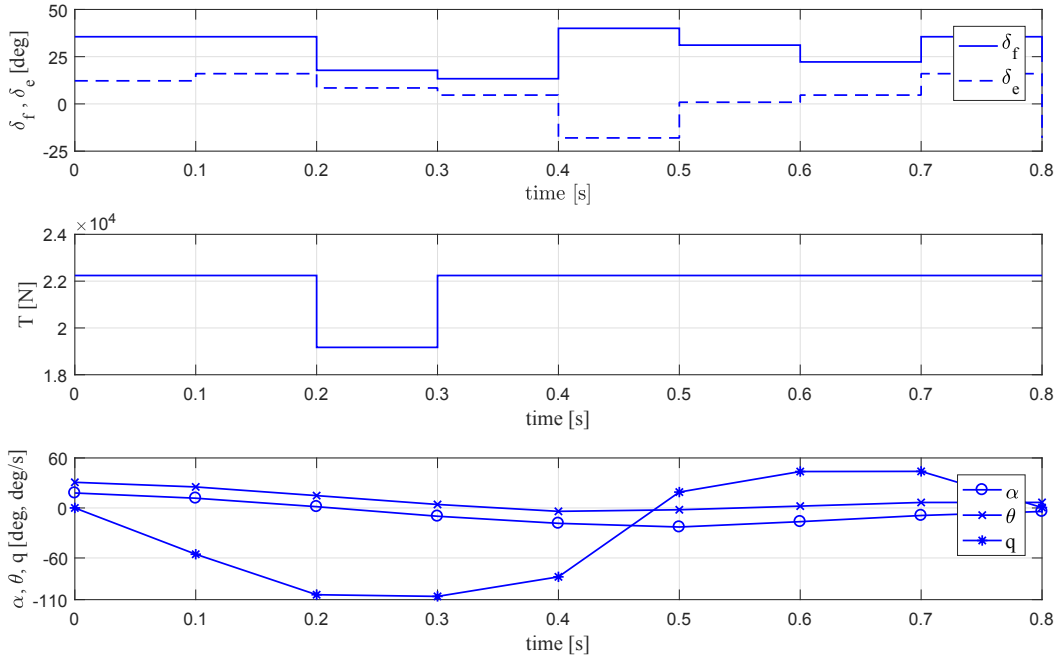

Fig. 20 Control input variation and state trajectory initialized at $(\alpha, \theta, q) = \left(18\frac{\pi}{180}\text{ rad}, 31\frac{\pi}{180}\text{ rad}, 0\text{ rad/s}\right)$ at Mach 0.4, sea level – Monte Carlo analysis for backward reachable set, nominal Cessna Citation II

VI. Lateral Envelope

Roll, yaw and sideslip define the lateral motion of an aircraft. The state variables that characterize the lateral motion are: velocity V, sideslip β, roll rate p, yaw rate r and roll angle ϕ. Since no longitudinal motion is involved, $q = \dot{q} = 0$, whereas the angle of attack α and the pitch angle θ are fixed with $\dot{\alpha} = \dot{\theta} = 0$. With these conditions, Eqs. 7, 8 and 9 can be reduced to lateral equations of motion:

$$\begin{cases} \dot{V} = \dfrac{1}{m}\left(T\cos\alpha\cos\beta - \frac{1}{2}\rho V^2 S C_D(\alpha) + mg_1\right) \\ \dot{\beta} = p\sin\alpha - r\cos\alpha + \dfrac{1}{mV}\left[-T\cos\alpha\sin\beta + \frac{1}{2}\rho V^2 S C_Y(\alpha,\beta,p,\delta_r) + mg_2\right] \\ \dot{p} = \dfrac{1}{J_{xx}J_{zz} - J_{zx}^2}\left(J_{zz}\frac{1}{2}\rho V^2 S b C_l(\alpha,\beta,p,r,\delta_a,\delta_r) + J_{zx}\frac{1}{2}\rho V^2 S b C_n(\alpha,\beta,p,r,\delta_a,\delta_r)\right) \\ \dot{r} = \dfrac{1}{J_{xx}J_{zz} - J_{zx}^2}\left(J_{zx}\frac{1}{2}\rho V^2 S b C_l(\alpha,\beta,p,r,\delta_a,\delta_r) + J_{xx}\frac{1}{2}\rho V^2 S b C_n(\alpha,\beta,p,r,\delta_a,\delta_r)\right) \\ \dot{\phi} = p + r\frac{\sin\theta}{\cos\theta}\cos\phi \end{cases} \tag{25}$$

In the above set of equations, g_1 and g_2 are the components of the gravity vector as were presented in section III.

A. Lateral Trim Envelope

The lateral trim envelope is computed by minimizing the following cost function for some fixed states:

$$J = W_V \dot{V}^2 + W_\beta \dot{\beta}^2 + W_p \dot{p}^2 + W_r \dot{r}^2 + W_\phi \dot{\phi}^2 \tag{26}$$

For the current research, a one dimensional (β) trim envelope has been computed with $p = r = \phi = 0$ at fixed longitudinally trimmed angle of attack α_{trim} and pitch angle θ_{trim} (straight level flight), see Table 4. The parameters for the lateral trim envelope computation for the Cessna Citation II are listed in Table 5. Sideslip angle is considered trimmed, if the inputs are within the bounds and the following conditions are satisfied:

$$\begin{gathered} \left|\dot{V}\right| \leq 1 \times 10^{-4}\ [\mathrm{m/s^2}], \quad \left|\dot{\beta}\right| \leq 5 \times 10^{-3}\ [\mathrm{rad/s}], \\ |\dot{p}| \leq 1 \times 10^{-4}\ [\mathrm{rad/s^2}], \quad |\dot{r}| \leq 1 \times 10^{-4}\ [\mathrm{rad/s^2}], \quad \left|\dot{\phi}\right| \leq 1 \times 10^{-4}\ [\mathrm{rad/s}] \end{gathered} \tag{27}$$

Table 4 Longitudinal trim states used for lateral trim computation

Flight Condition	$(\alpha_{trim}, \theta_{trim})$ [rad]
Mach 0.2, Sea level	$\left(0.286\frac{\pi}{180}, 5.73\frac{\pi}{180}\right)$
Mach 0.3, Sea level	$\left(-0.286\frac{\pi}{180}, 2.86\frac{\pi}{180}\right)$
Mach 0.4, Sea level	$\left(-1.43\frac{\pi}{180}, 0\frac{\pi}{180}\right)$
Mach 0.4, 5,000 m	$\left(-0.286\frac{\pi}{180}, 2.86\frac{\pi}{180}\right)$
Mach 0.4, 10,000 m	$\left(0.286\frac{\pi}{180}, 5.73\frac{\pi}{180}\right)$

Table 5 Parameters for the lateral trim envelope computation

Bounds	Grid Resolution	Cost Function Weights
$T \in [4448.2, 22241]$ [N] $\delta_a \in \left[-34\frac{\pi}{180}, 34\frac{\pi}{180}\right]$ [rad] $\delta_r \in \left[-22\frac{\pi}{180}, 22\frac{\pi}{180}\right]$ [rad] $\beta \in \left[-20\frac{\pi}{180}, 20\frac{\pi}{180}\right]$ [rad] $p = r = 0$ [rad/s] $\phi = 0$ [rad]	$\beta_{res} = 0.007$ [rad]	$W_V = W_\beta = W_p = W_r = W_\phi = 10$

The trimmed sideslip angle for the nominal Cessna Citation II at various flight conditions is presented in Figure 21. Similarly, Figure 22 shows a comparison of lateral trim set for different damage cases at Mach 0.4 at sea level. No major change is observed, either with the flight condition or with the vertical tail damage. However, a slight decrease can be noticed in the trim set for the damaged Cessna Citation II with 75% vertical tail loss. The almost unvarying behavior of the trim set with the vertical tail damage is due to the fact that although the rudder control effectiveness is

decreasing with the spanwise damage to the vertical tail, the side force Y generated by the sideslip is also decreasing, allowing the aircraft to trim at almost the same sideslip angle.

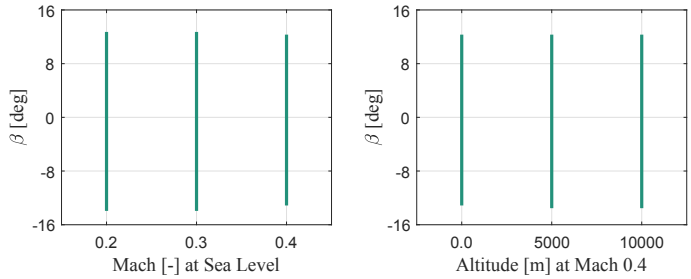

Fig. 21 Lateral trim set for nominal Cessna Citation II at various flight conditions

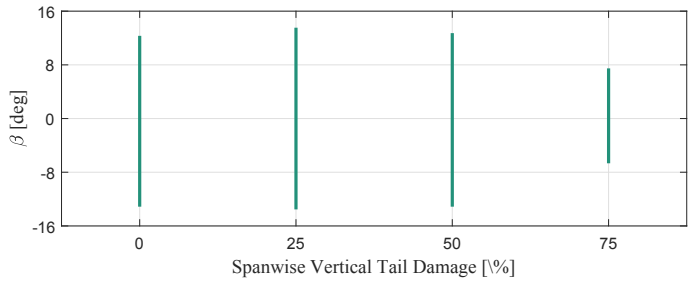

Fig. 22 Effects of vertical tail damage on lateral trim set for Cessna Citation II at Mach 0.4, sea level

Figure 23 present the variation in control inputs for trimming the aircraft laterally at various flight conditions. Similarly, Figure 24 shows the control input variation for trimming the damaged aircraft. It is interesting to see that the behavior of rudder deflection is reversed around 50% of vertical tail damage. This result is consistent with the result presented in Figure 11. The aircraft becomes laterally unstable around 50% of vertical tail damage and hence an opposite rudder deflection is required. In both figures, thrust and control deflection limits are shown with dotted lines.

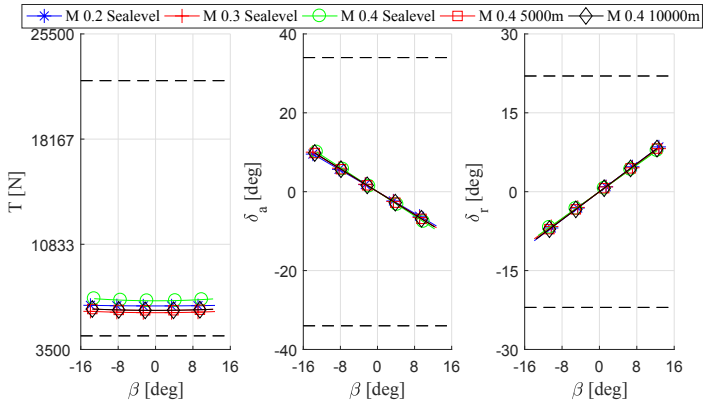

Fig. 23 Control input variation for lateral trim envelope for nominal Cessna Citation II

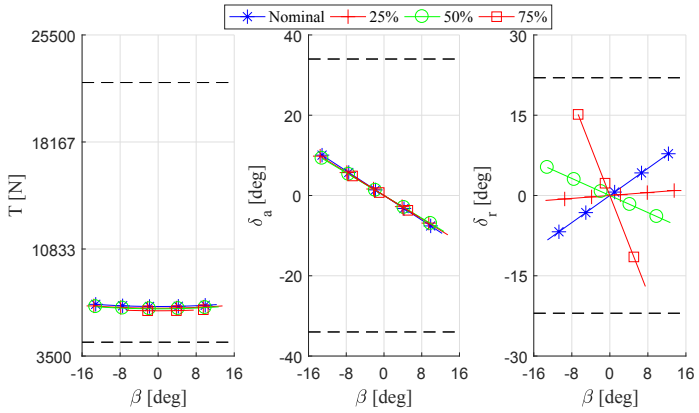

Fig. 24 Control input variation for lateral trim envelope for damaged Cessna Citation II at M 0.4, Sea level

B. Lateral Safe Flight Envelope

A two dimensional $(\beta - r)$ safe flight envelope is computed with $\dot{p} = p = \dot{\phi} = \phi = 0$ by evolving the trim set K forward and backwards in time. By considering the states in the proximity of $r = 0$ rad/s to be part of the trim set i.e., $\{r \in K \,|\, |r| \leq 0.01 \text{ rad/s}\}$, the following implicit function is defined:

$$l(\mathbf{x}) = \min\{x_1 - \beta_{min}, \beta_{max} - x_1, x_2 - r_{min}, r_{max} - x_2\} \tag{28}$$

Here as well, it can be noticed that $l(\mathbf{x}) \geq 0$ for $\mathbf{x} \in K$ and $l(\mathbf{x}) < 0$ for $\mathbf{x} \notin K$. Table 6 outlines the parameters that are assigned for the two dimensional reachable set computation.

Table 6 Solver settings for the reachable set computation (lateral safe flight envelope)

Parameter	Setting
Computational Domain	$\left[-60\frac{\pi}{180}, 60\frac{\pi}{180}\right]$ rad $\times$ $\left[-57.3\frac{\pi}{180}, 57.3\frac{\pi}{180}\right]$ rad/s
Number of Grid points	200×200
Time Horizon	1.0 s

The Hamiltonian function in Eq. 6 for the lateral safe flight envelope computation is defined as:

$$H(\mathbf{p}, \mathbf{x}, \mathbf{u}) = p_1\dot{\beta} + p_2\dot{r} \tag{29}$$

where the co-states in the above equation are: $p_1 = \frac{\partial V_2}{\partial \beta}$ and $p_2 = \frac{\partial V_2}{\partial r}$. With the aileron deflection δ_a being varied to prevent the aircraft from rolling and thrust T to maintain the constant velocity, the only minimizer in the Hamiltonian function in Eq. 29 is the rudder deflection δ_r, which yields the following quantity to be minimized in the Hamiltonian function:

$$p_1 \frac{\rho S}{2m} V C_{Y_{\delta_r}} \delta_r + p_2 \frac{\rho S b}{2\left(J_{xx}J_{zz} - J_{zx}^2\right)} V^2 \left(J_{zx}C_{l_{\delta_r}} + J_{xx}C_{n_{\delta_r}}\right) \delta_r \tag{30}$$

Then the optimal rudder deflection to minimize the Hamiltonian function becomes straightforward:

$$\bullet\ \delta_r = \begin{cases} \delta_{r_{min}} & \text{if } p_1 \frac{\rho S}{2m} V C_{Y_{\delta_r}} + p_2 \frac{\rho S b}{2\left(J_{xx}J_{zz} - J_{zx}^2\right)} V^2 \left(J_{zx} C_{l_{\delta_r}} + J_{xx} C_{n_{\delta_r}}\right) > 0 \\ \delta_{r_{max}} & \text{if } p_1 \frac{\rho S}{2m} V C_{Y_{\delta_r}} + p_2 \frac{\rho S b}{2\left(J_{xx}J_{zz} - J_{zx}^2\right)} V^2 \left(J_{zx} C_{l_{\delta_r}} + J_{xx} C_{n_{\delta_r}}\right) < 0 \\ \left[\delta_{r_{min}}, \delta_{r_{max}}\right] & \text{if } p_1 \frac{\rho S}{2m} V C_{Y_{\delta_r}} + p_2 \frac{\rho S b}{2\left(J_{xx}J_{zz} - J_{zx}^2\right)} V^2 \left(J_{zx} C_{l_{\delta_r}} + J_{xx} C_{n_{\delta_r}}\right) = 0 \end{cases}$$

The required aileron deflection δ_a to keep the aircraft level is computed by setting $\dot{p} = 0$ in Eq. 25 and solving for δ_a. Moreover, the required thrust T is computed by setting $\dot{V} = 0$ in Eq. 25 and solving for T.

Figures 25 and 26 show the variation of the lateral safe flight envelope with different flight conditions for the nominal aircraft. As expected, the safe flight envelope grows as the velocity of the aircraft increases, shown in Figure 25. Additionally, the safe flight envelope shrinks as the altitude increases from sea level to 10,000 m, see Figure 26.

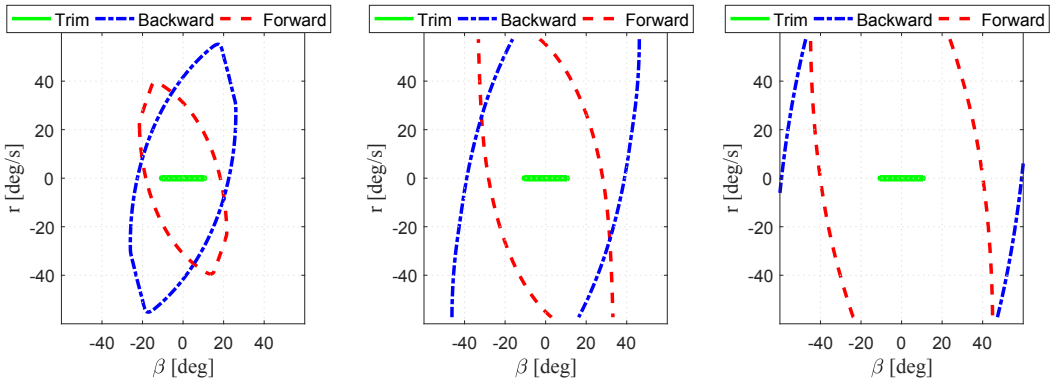

(a) Mach 0.2; sea level (b) Mach 0.3; sea level (c) Mach 0.4; sea level

Fig. 25 Lateral safe flight envelope for nominal Cessna Citation II with $T = 1$ s (variation with Mach number)

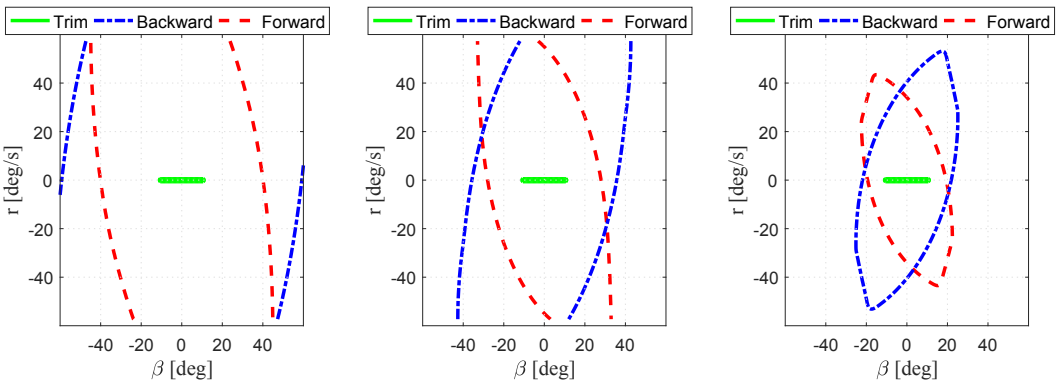

(a) Mach 0.4; sea level (b) Mach 0.4; 5,000 m (c) Mach 0.4; 10,000 m

Fig. 26 Lateral safe flight envelope for nominal Cessna Citation II with $T = 1$ s (variation with altitude)

Figure 27 shows the lateral safe flight envelopes for Cessna Citation II for various vertical tail damages at Mach 0.4 at sea level. As the percentage of spanwise vertical tail damage increases, the safe flight envelope shrinks. The range

of sideslip angle in the forward and the backward reachable sets decreases with the vertical tail damage. However, the yaw rate range is almost the same for various damages. This shrinking in the safe flight envelope is unlike the shrinking in the safe flight envelope due to different flight conditions. At higher altitudes and lower Mach numbers, the overall maneuvering capability of the aircraft decreases and the aircraft cannot simply reach high sideslip angles and high yaw rates. On the contrary, due to spanwise vertical tail damage the aircraft can reach to or comeback from high sideslip angles but at high yaw rates.

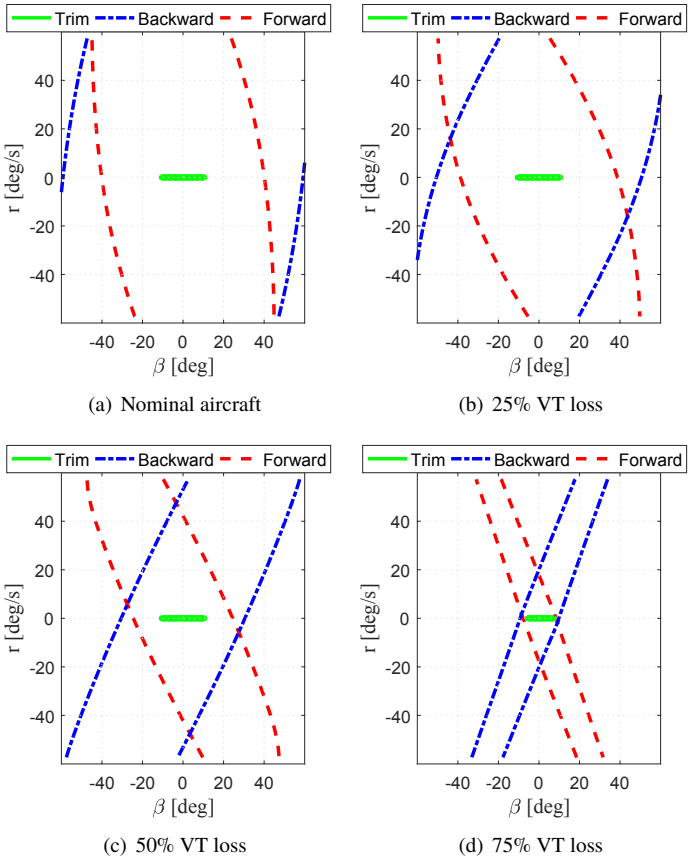

(a) Nominal aircraft (b) 25% VT loss

(c) 50% VT loss (d) 75% VT loss

Fig. 27 Comparison of lateral safe flight envelopes for nominal and damaged Cessna Citation II with $T = 1$ s at Mach 0.4, sea level

Lastly, Figure 28 presents the safe flight envelopes for the nominal Cessna Citation II at Mach 0.4 at sea level for three different time horizons. As the time horizon decreases, the lateral safe flight envelope shrinks in $\beta-$axis i.e., a limited range of sideslip angle is reachable with almost same yaw rate, unlike the safe flight envelope for the damaged vertical tail where higher sideslip angles were reachable, however, at higher yaw rates.

The changes in the lateral safe flight envelope due to different flight conditions, vertical tail damages and time horizons are summarized in Figure 29. With different flight conditions, the change in the lateral safe flight envelope has the same behavior as in the longitudinal safe flight envelope i.e., the safe flight envelope changes almost linearly

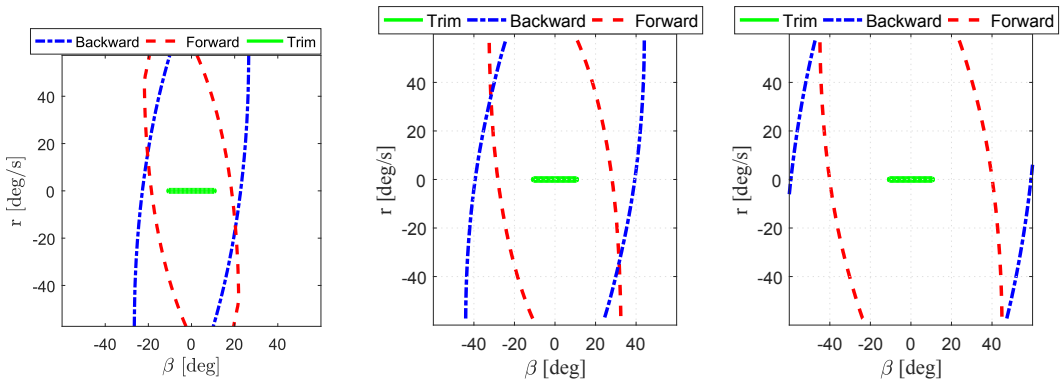

(a) T = 0.5 s (b) T = 0.75 s (c) T = 1.0 s

Fig. 28 Lateral safe flight envelope for nominal Cessna Citation II at Mach 0.4, sea level (variation with time horizon)

with different flight conditions as suggested by the results presented in the top two plots of Figure 29. Figure 29(c) shows that the reachable set expands linearly with increasing time horizon T. The shrinkage in the reachability sets with the vertical tail damage is shown in Figure 29(d). The percentage of grid points inside the reachable set decreases with increasing spanwise vertical tail damage, however, the change is not linear.

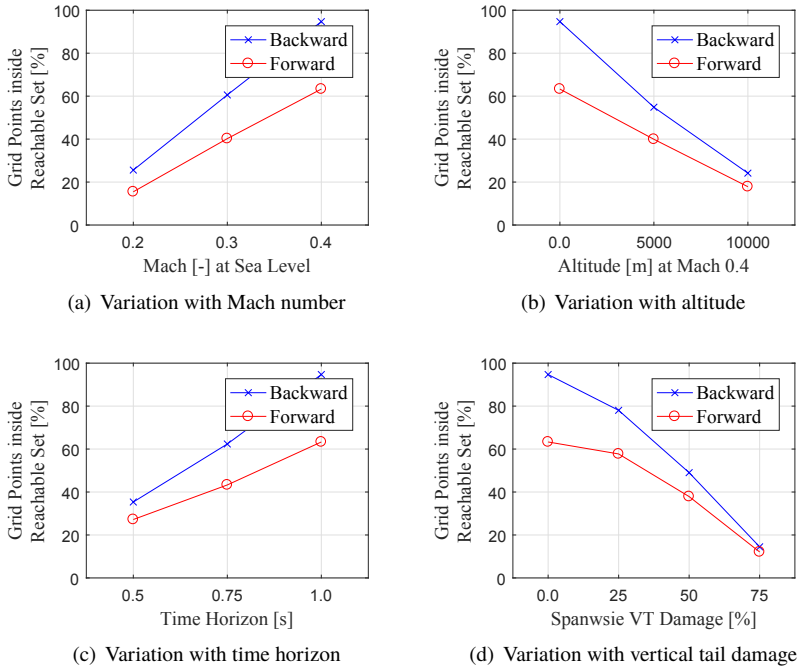

(a) Variation with Mach number (b) Variation with altitude

(c) Variation with time horizon (d) Variation with vertical tail damage

Fig. 29 Change in the percentage of grid points inside the lateral reachable set

In order to demonstrate the feasibility of the database approach, the variation of the number of grid points inside the reachable set with Mach number and altitude has been fit with a linear model. One trial Mach number and one

altitude level is investigated. Table 7 presents the comparison between the actual and the approximated number of grid points inside the reachable set. The results obtained from linear model and level set method are quite comparable and the premise of interpolation between flight conditions within the database has been verified.

Table 7 Comparison of level set method and interpolation with linear model for nominal Cessna Citation II with $T = 1$ s for two different flight conditions

Flight Condition	Reachability Set	No. of Grid Points inside Reachable Set		Error
		Actual	1st Order Approx.	
Mach 0.35, Sea Level	Forward	20966	20646	-1.53 %
	Backward	31922	31018	-2.83 %
Mach 0.4, 7500 m	Forward	11062	11598	4.84 %
	Backward	15380	16105	4.7 %

Similarly, variation of the number of grid points inside the reachable set with spanwise vertical tail damage, Figure 29(d), has been fit with a quadratic polynomial model. Two spanwise vertical tail damages are investigated in order to substantiate the hypothesis of interpolatibility. Table 8 shows the comparison between the number of grid points inside the reachable set computed using the level set method and the second order polynomial interpolation. For both damages, it can be seen that the quadratic polynomial interpolation has approximated the number of grid points inside the reachable set fairly close to the actual results obtained by the level set method for both backward and forward reachable sets. The idea of interpolation in the database approach is corroborated by the comparison presented in Tables 7 and 8. One important thing to note here is that a successful implementation of the database approach requires an online detection and isolation of faults and damages. This is part of the ongoing research [15–17].

Table 8 Comparison of level set method and interpolation with quadratic polynomial model at Mach 0.4, sea level with $T = 1$ s for two damage scenarios

Damage Type	Reachability Set	No. of Grid Points inside Reachable Set		Error
		Actual	2nd Order Approx.	
40% VT Lost	Forward	17882	18912	5.76 %
	Backward	23208	24759	6.68 %
60% VT Lost	Forward	11976	11745	-1.9 %
	Backward	15306	14699	-3.9 %

VII. Conclusion

In order to investigate the feasibility of the novel database approach for online flight envelope prediction, three dimensional longitudinal and two dimensional lateral safe flight envelopes for the nominal and the damaged Cessna Citation II at various flight conditions are computed and presented in this paper. For the purpose of decoupling the

dynamics, symmetrical damages with spanwise vertical tail damage are considered.

The safe flight envelopes are computed by defining a nonlinear reachability problem and solving it with the level set method through an optimal control formulation using actual aircraft control surface inputs. A nonlinear reachability analysis is based on the physical model of an aircraft. Therefore, a simple method to compute the physical parameters of the damaged aircraft (mass, inertia etc.) is presented. Moreover, the aerodynamic stability and control derivatives are calculated using Digital Datcom.

It is shown that, although the principle of timescale separation is very useful to solve the problem of "curse of dimensionality" in the reachability analysis for the slower dynamics, it is not feasible to implement the same principle for the reachability computation for faster dynamics when considering the aircraft control surfaces as inputs.

By analyzing both longitudinal and lateral safe flight envelopes, it is observed that the reachability set extends far beyond the region where the linear aerodynamic model and the structural limits are valid. Introducing the aerodynamic model and structural limits will help restrict the computational domain. Moreover, it is also observed that the reachability analysis computes a safe flight envelope that is "theoretically" reachable, however, practically it might not be possible to reach such a state due to high rate of control input or the maneuver requirement, that is out of pilot's bandwidth or exceeds the actuator dynamics limits. It is proposed that the fidelity of the simulation can be improved and realistic safe flight envelopes can be obtained by incorporating the actuator dynamics and pilot model in the safe flight envelope computation.

It is demonstrated that the flight conditions have same effect on the longitudinal and the lateral safe flight envelopes. The safe flight envelope expands almost linearly with increasing Mach number while it shrinks linearly with increasing altitude. This result is consistent with the fact that with an increasing dynamic pressure, the maneuverability of an aircraft increases, whereas the maneuverability decreases with increasing altitude. Similarly, the effects of various time horizons on the safe flight envelope are also presented. It is shown that the safe flight envelope grows as the time horizon is increased.

Furthermore, the lateral safe flight envelopes for Cessna Citation II with 0%, 25%, 50% and 75% vertical tail losses are compared. The comparison is quantified by the number of grid points inside the backward and the forward reachable sets. The results show that the number of grid points inside the reachable set declines almost quadratically with increasing spanwise vertical tail damage. A second order polynomial model is fitted on this data and then two candidate vertical tail damages are interpolated using this quadratic polynomial model. The same idea of interpolation is also verified for different flight conditions by using a linear regression model. The comparison between the actual and the approximated grid points inside the reachable set shows promising results and supports the hypothesis of interpolatibility in the database approach.

It is further demonstrated that different flight conditions, various time horizons and the vertical tail damages have different effects on the safe flight envelope. However, a unique trend can be observed for each of these categories.

At this moment, only the symmetrical damages are considered. Future work will extend to asymmetrical damages. It should be noted, however, that in case of asymmetrical damages, the decomposition of the flight dynamics into longitudinal and lateral dynamics will no be longer valid and a nine dimensional safe flight envelope will have to be computed. Therefore, a more computationally efficient method, such as minimal time schemes, has to be explored such that the higher dimensional safe flight envelopes can be computed offline and a database of these safe flight envelopes for various damages at different flight conditions can be constructed and analyzed. Furthermore, in order to compute a more realistic safe flight envelope, consideration of robustness in physical parameters (mass and inertia, aerodynamic derivatives etc.) along with atmospheric disturbances will be taken into account in the subsequent research. Additionally, system dynamics will be modified by implementing the rate constraints on the control inputs and actuators to improve the fidelity of computed safe flight envelopes. Moreover, future work will also include extensive and in-depth research in physical modeling (mass and inertia model, aerodynamic model etc.) of the damaged aircraft. Another important topic of the ongoing research is the damage and failure identification and classification.

References

[1] Boeing, "Statistical Summary of Commercial Jet Airplane Accidents - Worldwide Operations 1959 - 2015," Technical report, Aviation Safety, Boeing Commercial Airplanes, Seattle, WA 98124-2207, 2016. URL `http://www.boeing.com/news/techissues/pdf/statsum.pdf`.

[2] Kwatny, H. G., Dongmo, J.-E. T., Chang, B.-C., Bajpai, G., Yasar, M., and Belcastro, C., "Nonlinear Analysis of Aircraft Loss of Control," *Journal of Guidance, Control and Dynamics*, Vol. 36, No. 1, 2013, pp. 149–162. doi:10.2514/1.56948.

[3] Lopez, I., and Sarigul-Klijn, N., "A review of uncertainty in flight vehicle structural damage monitoring, diagnosis and control: Challenges and opportunities," *Progress in Aerospace Sciences*, Vol. 46, No. 7, 2010, pp. 247–273. doi:10.1016/j.paerosci.2010.03.003.

[4] Lombaerts, T. J. J., "Fault Tolerant Flight Control - A Physical Model Approach," Ph.D. dissertation, Faculty of Aerospace Engineering, Delft University of Technology, May 2010. URL `http://repository.tudelft.nl/view/ir/uuid%3A538b0174-fe84-43af-954d-02f256b2ec50/`.

[5] Stroosma, O., Smaïli, H., Lombaerts, T., and Mulder, J. A., "Piloted Simulator Evaluation of New Fault-Tolerant Flight Control Algorithms for Reconstructed Accident Scenarios," *AIAA Modeling and Simulation Technologies Conference and Exhibit*, 2008. doi:10.2514/6.2008-6534.

[6] Lombaerts, T., Schuet, S., Acosta, D. M., Kaneshige, J., Shish, K. H., and Martin, L., "Piloted Simulator Evaluation of Maneuvering Envelope Information for Flight Crew Awareness," *AIAA Guidance, Navigation, and Control Conference, AIAA SciTech*, 2015. doi:10.2514/6.2015-1546.

[7] Goman, M. G., Khramtsovsky, A. V., and Kolesnikov, E. N., "Evaluation of Aircraft Performance and Maneuverability by

Computation of Attainable Equilibrium Sets," *Journal of Guidance, Control and Dynamics*, Vol. 31, No. 2, 2008, pp. 329–339. doi:10.2514/1.29336.

[8] Keller, J. D., McKillip, R. M., and Kim, S., "Aircraft Flight Envelope Determination using Upset Detection and Physical Modeling Methods," *AIAA Guidance, Navigation, and Control Conference*, 2009. doi:10.2514/6.2009-6259.

[9] Menon, P. K., Sengupta, P., Vaddi, S., Yang, B.-J., and Kwan, J., "Impaired Aircraft Performance Envelope Estimation," *Journal of Aircraft*, Vol. 50, No. 2, 2013, pp. 410–424. doi:10.2514/1.C031847.

[10] Kitsios, I., and Lygeros, J., "Launch-Pad Abort Flight Envelope Computation for a Personnel Launch Vehicle Using Reachability," *AIAA Guidance, Navigation, and Control Conference and Exhibit*, 2005. doi:10.2514/6.2005-6150.

[11] Seube, N., and Moitie, R., "Viability Analysis of an Aircraft Flight Domain for Take-Off in a Windshear," *Mathematical and Computer Modelling*, Vol. 36, No. 6, 2002, pp. 633–641. doi:10.1016/S0895-7177(02)00164-4.

[12] van Oort, E. R., Chu, Q. P., and Mulder, J. A., "Maneuver Envelope Determination through Reachability Analysis," *Advances in Aerospace Guidance, Navigation and Control: Selected Papers of the 1st CEAS Specialist Conference on Guidance, Navigation and Control*, Springer Berlin Heidelberg, 2011, pp. 91–102. doi:10.1007/978-3-642-19817-5_8.

[13] Stapel, J. C. J., de Visser, C. C., Chu, Q. P., and van Kampen, E., "Efficient Methods for Flight Envelope Estimation through Reachability Analysis," *AIAA Guidance, Navigation, and Control Conference, AIAA SciTech*, 2016. doi:10.2514/6.2016-0083.

[14] Tang, L., Roemer, M., Ge, J., Crassidis, A., Prasad, J. V. R., and Belcastro, C., "Methodologies for Adaptive Flight Envelope Estimation and Protection," *AIAA Guidance, Navigation, and Control Conference*, 2009. doi:10.2514/6.2009-6260.

[15] Zhang, Y., de Visser, C. C., and Chu, Q. P., "Online Safe Flight Envelope Prediction for Damaged Aircraft: A Database-driven Approach," *AIAA Modeling and Simulation Technologies Conference, AIAA SciTech*, 2016. doi:10.2514/6.2016-1189.

[16] Zhang, Y., de Visser, C. C., and Chu, Q. P., "Online Physical Model Identification for Database-driven Safe Flight Envelope Prediction of Damaged Aircraft," *AIAA Atmospheric Flight Mechanics Conference, AIAA SciTech*, 2016. doi:10.2514/6.2016-2011.

[17] Zhang, Y., de Visser, C. C., and Chu, Q. P., "Aircraft Damage Identification and Classification for Database-driven Online Safe Flight Envelope Prediction," *AIAA Atmospheric Flight Mechanics Conference, AIAA SciTech*, 2017. doi:10.2514/6.2017-1863.

[18] Anderson, J. D., *Aircraft Performance and Design*, 1st ed., McGraw-Hill Education, 1998.

[19] Ruijgrok, G. J. J., *Elements of Airplane Performance*, 2nd ed., Delft University Press, 2007.

[20] van Oort, E. R., "Adaptive Backstepping Control and Safety Analysis for Modern Fighter Aircraft," Ph.D. dissertation, Faculty of Aerospace Engineering, Delft University of Technology, June 2011. URL `http://repository.tudelft.nl/view/ir/uuid%3A68fd89ff-aad6-4ad8-b280-d2fe8b500d48/`.

[21] Lygeros, J., "On Reachability and Minimum Cost Optimal Control," *Automatica*, Vol. 40, No. 6, 2004, pp. 917–927. doi: 10.1016/j.automatica.2004.01.012.

[22] Mitchell, I., and Tomlin, C. J., "Level Set Methods for Computation in Hybrid Systems," *Hybrid Systems: Computation and Control, Lecture Notes in Computer Science*, Vol. 1790, 2000, pp. 310–323. doi:10.1007/3-540-46430-1_27.

[23] Mitchell, I., Bayen, A. M., and Tomlin, C. J., "Validating a Hamilton-Jacobi Approximation to Hybrid System Reachable Set," *Hybrid Systems: Computation and Control, Lecture Notes in Computer Science*, Vol. 2034, 2001, pp. 418–432. doi: 10.1007/3-540-45351-2_34.

[24] Osher, S., and Fedkiw, R., *Level Set Methods and Dynamic Implicit Surfaces*, 1st ed., Applied Mathematical Sciences, Vol. 153, Springer-Verlag New York, 2003. doi:10.1007/b98879.

[25] Bayen, A. M., Mitchell, I. M., Osihi, M. K., and Tomlin, C. J., "Aircraft Autolander Safety Analysis Through Optimal Control-Based Reach Set Computation," *Journal of Guidance, Control and Dynamics*, Vol. 30, No. 1, 2007, pp. 68–77. doi:10.2514/1.21562.

[26] Schuet, S., Lombaerts, T., Acosta, D., Wheeler, K., and Kaneshige, J., "An Adaptive Nonlinear Aircraft Maneuvering Envelope Estimation Approach for Online Applications," *AIAA Guidance, Navigation, and Control Conference, AIAA SciTech*, 2014. doi:10.2514/6.2014-0268.

[27] Lombaerts, T. J. J., Schuet, S. R., Wheeler, K. R., Acosta, D. M., and Kaneshige, J. T., "Safe Maneuvering Envelope Estimation Based on a Physical Approach," *AIAA Guidance, Navigation, and Control Conference*, 2013. doi:10.2514/6.2013-4618.

[28] Marco, A. D., Duke, E. L., and Berndt, J. S., "A General Solution to the Aircraft Trim Problem," *AIAA Modeling and Simulation Technologies Conference and Exhibit*, 2007. doi:10.2514/6.2007-6703.

[29] Yi, G., and Atkins, E. M., "Methods of Trim State Discovery," *3rd International Symposium on Systems and Control in Aeronautics and Astronautics (ISSCAA)*, 2010, pp. 654 – 659. doi:10.1109/ISSCAA.2010.5633238.

[30] Elgersma, M. R., and Morton, B. G., "Nonlinear Six-Degree-of-Freedom Aircraft Trim," *Journal of Guidance, Control and Dynamics*, Vol. 23, No. 2, 2000, pp. 305–311. doi:10.2514/2.4523.

[31] van Kampen, E., Chu, Q. P., Mulder, J. A., and van Emden, M. H., "Nonlinear Aircraft Trim using Interval Analysis," *AIAA Guidance, Navigation, and Control Conference and Exhibit*, 2007. doi:10.2514/6.2007-6766.

[32] Ananthkrishnan, N., and Sinha, N. K., "Level Flight Trim and Stability Analysis using Extended Bifurcation and Continuation Procedure," *Journal of Guidance, Control and Dynamics*, Vol. 24, No. 6, 2001, pp. 1225–1228. doi:10.2514/2.4839.

[33] Stevens, B. L., and Lewis, F. L., *Aircraft Control and Simulation*, 2nd ed., Wiley-Interscience Publication, 2003.

[34] Shah, G. H., "Aerodynamic Effects and Modeling of Damage to Transport Aircraft," *AIAA Atmospheric Flight Mechanics Conference and Exhibit*, 2008. doi:10.2514/6.2008-6203.

[35] Bacon, B. J., and Gregory, I. M., "General Equations of Motion for a Damaged Asymmetric Aircraft," *AIAA Atmospheric Flight Mechanics Conference and Exhibit*, 2007. doi:10.2514/6.2007-6306.

[36] Williams, J. E., and Vukelich, S. R., "The USAF Stability and Control Digital Datcom, Volume I, Users Manual," Technical Report AFFDL-TR-79-3032 (AD A086557), Flight Controls Division, Air Force Flight Dynamics Laboratory, Wright-Patterson Air Force Base, Ohio 45433, April 1979. URL `http://www.pdas.com/datcomrefs.html`.

[37] Sadraey, M. H., *Aircraft Design: A Systems Engineering Approach*, 1st ed., Aerospace Series, John Wiley & Sons, 2012.

[38] Finck, R. D., "USAF Stability and Control Datcom," Technical Report AFWAL-TR-83-3048, Flight Controls Division, Air Force Flight Dynamics Laboratory, Wright-Patterson Air Force Base, Ohio 45433, April 1978. URL `http://www.pdas.com/datcomrefs.html`.